NASA CR-111808

FLUIDIC WIND SENSOR RESEARCH LEADING TO A FLIGHT TEST MODEL

FINAL REPORT

R-11-13-70

by

V. F. Neradka

December 1970

Prepared Under Contract NAS 12-2257 by

BOWLES FLUIDICS CORPORATION
9347 Fraser Avenue
Silver Spring, Maryland 20910

for

NASA/LANGLEY RESEARCH CENTER
Hampton, Virginia 23365

ABSTRACT

Three tasks leading to the delivery of a flyable fluidic low speed wind sensor are discussed. These include a flow visualization study of the flow internal and external to the sensor with regard to velocity threshold and angular resolving capability. Based on the research, a flight-worthy model of a single axis sensor was fabricated and wind tunnel tested over the velocity range $-160 < V < 160$ ft/sec. Of particular interest is the linearity of the sensor for $V < 20$ ft/sec. Wind tunnel tests in a contaminated atmosphere were conducted and the unit continued to operate after several days in severe environments. A configuration for a model which measures air speed and direction over total spherical coordinates is presented.

LIST OF FIGURES

1.0 INTRODUCTION

The increasing interest in V/STOL aircraft has generated the need for instrumentation unique to the operation of these aircraft. The need has been acknowledged for research instrumentation, and it has additionally been demonstrated (Reference 1) that there is a definite optimum takeoff trajectory for helicopters, the computation of which requires precise low speed airspeed measurement.

The fluidic air speed sensor designed by the Bowles Fluidics Corporation under this contract fulfills the need for a practical instrument which measures the velocity in the V/STOL flight regime. This instrument is inherently rugged, reliable, accurate at low speeds, provides an output of sufficient magnitude for standard instrumentation and is compatible with crowded aircraft interiors. The fluidic sensor fills these specific requirements, and in addition, provides a capability to operate over an extended velocity range. The sensor is also capable of angular resolution of velocity.

Under a previous contract (NAS 12-2038), the Bowles Fluidics Corporation was engaged in basic research and development of a low speed air speed sensor. Two techniques were investigated in that program (Reference 2). They were designed as the "cross flow" and the "parallel flow" sensors.

1.1 Cross Flow Sensor

In the fluidic amplifier (Figure 1), flow emitted from the power nozzle (P_+) evenly divides between the two output legs of the amplifier. The output differential pressure is zero. Impressing a control pressure (P_{C_L}) upon the supply pressure deflects the supply flow toward one output leg of the amplifier and away from the other. The result is a differential pressure proportional to the control pressure.

Figure 2 shows this concept as applied to sensing wind speed. The difference between the basic amplifier and the wind sensor is that in the wind sensing embodiment, the control, which is the wind itself, acts over the entire length of the jet.

A unit of this type has also been extensively studied by others (References 3,4), and found to have a quadratic output characteristic due to its operation on momentum principles unless high supply pressure were employed. These high pressures give rise to high jet noise. Moreover, the cross flow sensor has a saturation velocity of 80 ft/sec (Reference 5) regardless of the supply pressure (contrary to intuition, which suggests that the saturated

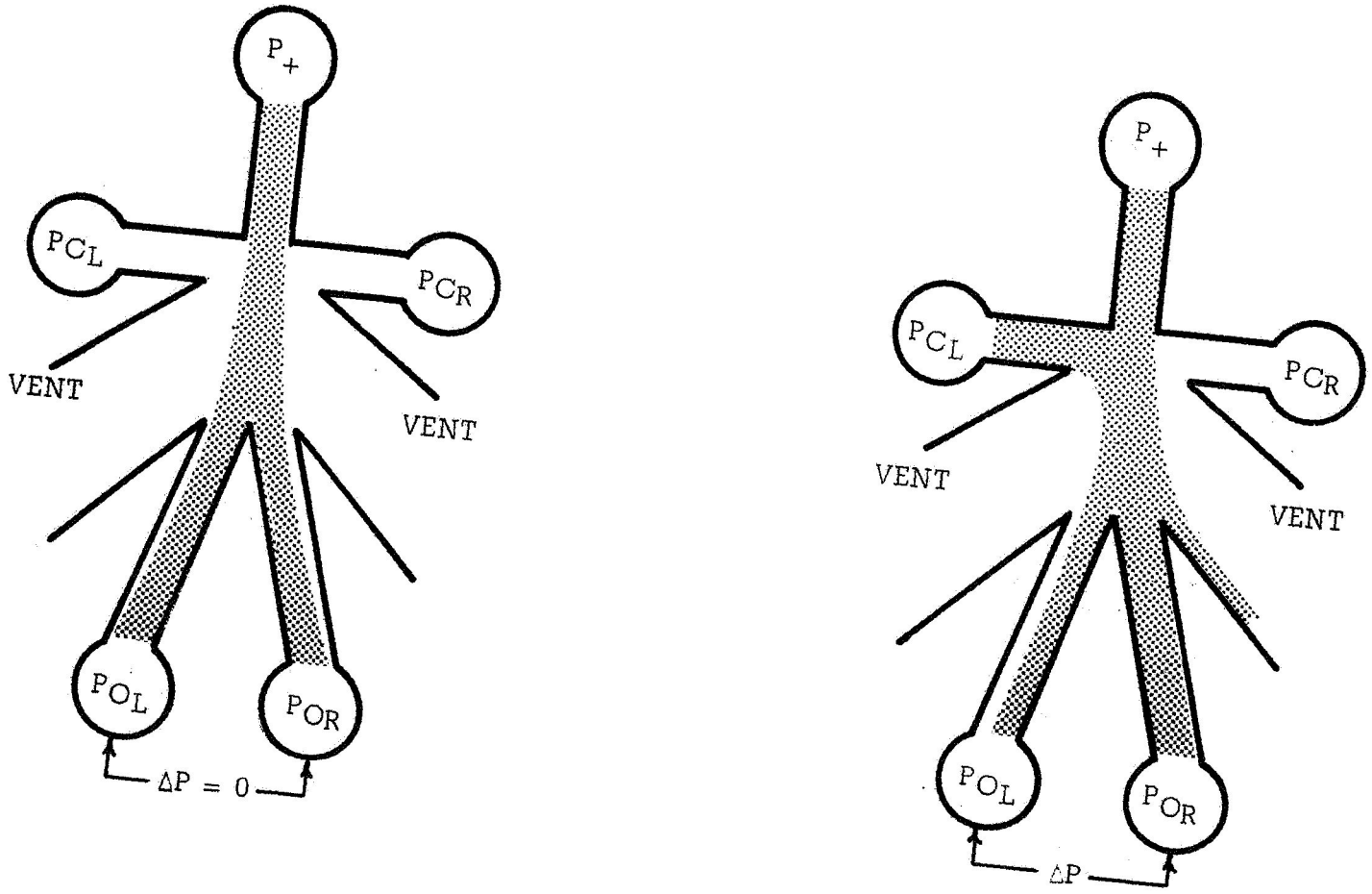

Figure 1.
FLUIDIC ANALOG AMPLIFIER

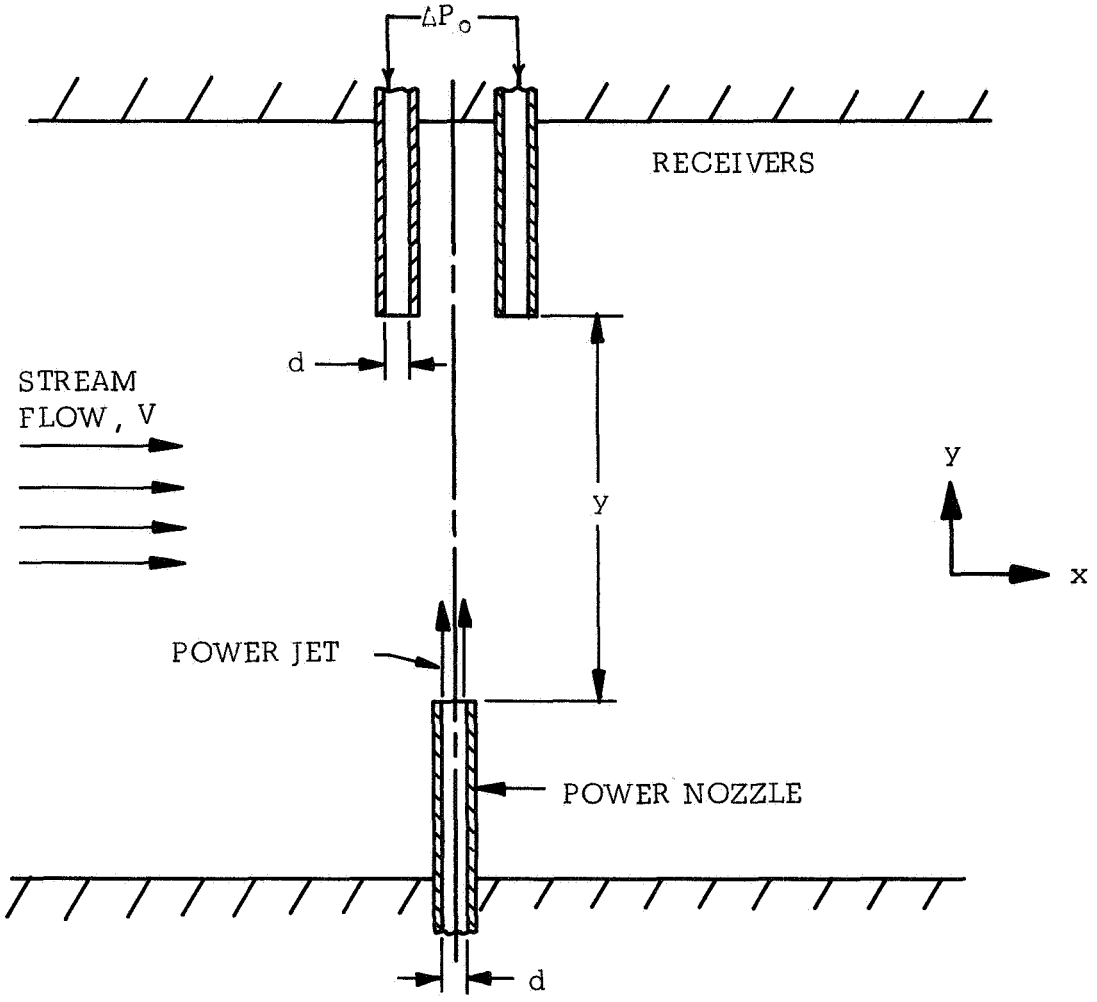

Figure 2.
CROSS FLOW SENSOR CONFIGURATION

jet may be returned to the vicinity of the receivers by increasing supply pressure.*) Because of the NASA-prescribed velocity range of 160 ft/sec and the tacit requirement of low power consumption, this approach was discarded for the more feasible parallel flow concept.

1.2 Parallel Flow Wind Sensor

The parallel flow concept, which is the basis for the design developed under this program, operates on a bridge-type principle where bridge unbalance is the result of viscous interaction between two air jets and the ambient air speed to be measured. The unit is shown schematically in Figure 3.

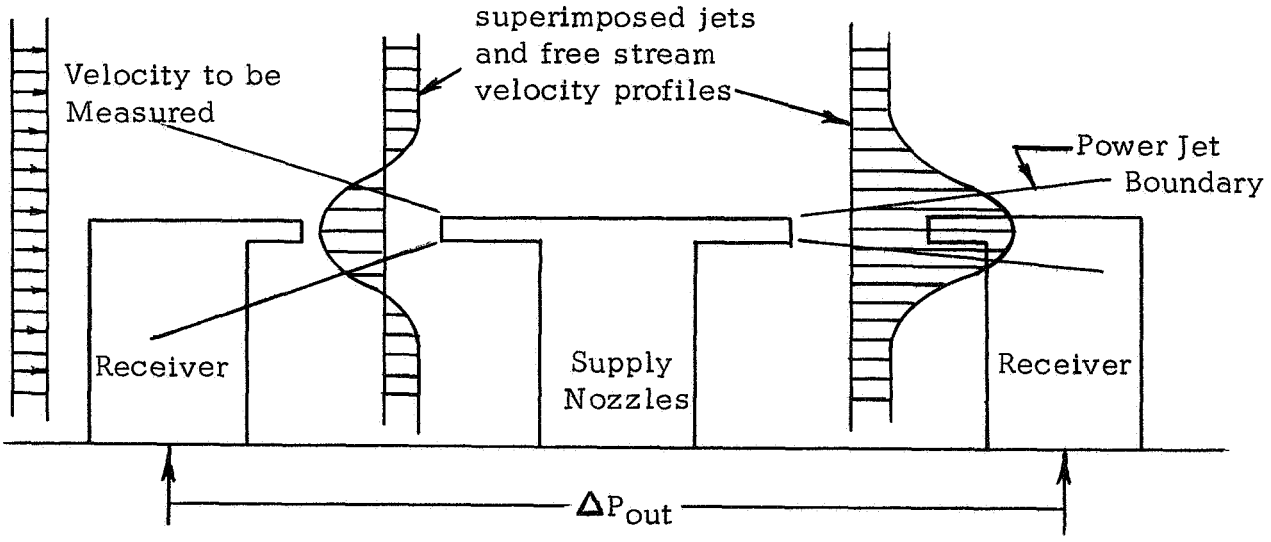

Figure 3.
PARALLEL FLOW SENSOR CONFIGURATION

Flow entering the power supply nozzles, P_+, divides evenly between two nozzles mounted on a common centerline. Separated from these nozzles at a fixed distance along the same centerline are two signal

*This has been demonstrated for low pressure closed loop operation of the wind sensor, Reference 2.

pressure receivers. By virtue of the difference in jet mixing in the power jet into and the power jet with the wind, a differential pressure is obtained.

The earliest work on this sensor showed that the unit was linear over the velocity range $1/4 < V < 160$ ft/sec. The data suggest that the sensor will operate at velocities much higher than 160 ft/sec, the maximum possible in the wind tunnel used for the testing. A low power consumption is an especially favorable feature of the unit. The early work brought to light a low frequency noise (i.e., pressure fluctuation) superimposed on the output pressure signal, and this formed a major portion of the work of the program reported here. This low frequency noise, if not eliminated, can be misinterpreted as gusty atmospheric weather conditions. A second effort of the recent program was to improve the output signal variation with angle of attack of the unit to permit multi-axis velocity measurement with no moving parts. Under the recent program, a single axis flight-worthy test model was built, complete with instrumentation package for flight test evaluation.

Funded under Navy Contract N00014-70-C-0338, the parallel flow sensor built under the Contract NAS 12-2038 was wind tunnel tested in adverse environments and found to operate in a predictable and repeatable manner in contaminated environments which would immediately disable many conventional sensors. Although not a part of the present program, these results are of sufficient importance to be included as an appendix to this report.

2.0 NOISE INVESTIGATION

The noise problem associated with the Fluidic air-speed sensor is particularly acute insofar as it is low frequency and therefore difficult to filter, either pneumatically or electronically. It is therefore necessary to reduce the inherent noise, i.e., that arising from the flowing fluid itself, as much as possible by proper aerodynamic design.

Because of the complexity of the flow patterns in a configuration such as the wind sensor (Figure 3), one must rely primarily on experimental rather than analytical techniques. Flow visualization is easily accomplished using water as the working fluid, injecting dye into the water at strategic locations and observing its subsequent path. Because the wind sensor is primarily intended for use at relatively low velocities compressibility effects of the air are insignificant, and dynamically similar flow patterns in air and water may be obtained by matching the Reynolds Number in both fluids (Reference 6), $R = \frac{Vd}{\nu}$ where

V = free stream velocity

d = cylinder diameter

ν = kinematic viscosity of the working fluid

Since the same model is to be used in both water and air, the free stream velocities are related by:

$$V_w = \frac{\nu_w}{\nu_a} V_a$$

Thus for 15 ft/sec wind speed in air, the corresponding water speed is nominally 1 ft/sec.

The Reynolds Number for a jet of fluid exhausting into its surroundings is (Reference 7):

$$R = \frac{2(P_+ d x)^{1/3}}{\rho^{1/3} \nu^{2/3}}$$

where P_+ = jet supply pressure

d = supply nozzle diameter

x = distance from power nozzle to receiver

ρ = fluid density

ν = fluid kinematic viscosity

Once again using the same model in both air and water, the condition for similarity ($R_a = R_w$) simplifies to:

$$1 = \left(\frac{P_{+a}}{P_{+w}}\right)\left(\frac{\rho_w}{\rho_a}\right)\left(\frac{\nu_w}{\nu_a}\right)^2$$

Introducing the physical properties of the fluids enables one to find the supply pressure necessary to insure similar jet flows, namely

$$\frac{P_{+w}}{P_{+a}} = 3.5$$

Thus to simulate 1 psi supply pressure in air (typical of the values used in previous work), 3.5 psi must be used in water.

A final aspect of the flow simulation of interest is the nonsteady nature of the signal, which arises from oscillations in the flow.

The frequency of an occurrence in water can be related to an occurrence in air by using the dimensionless frequency known as the Strouhal Number, $S = \omega d/V$ (Reference 6)

where ω = frequency of oscillation

d = nozzle diameter

V = fluid velocity

In using this, the Reynolds Number (as discussed above) must be matched, as $S = S(R)$. Equating Strouhal Numbers into two fluids (again using the same model in both fluids) yields

$$\frac{\omega_w}{\omega_a} = \frac{\nu_w}{\nu_a}$$

A 1 Hz motion in water corresponds to approximately 15 Hz motion in air.

It is thus demonstrated that the flow of air over and through the wind sensor can be simulated by the flow of water using an identical model. The advantages of using water are:

1. Economy
2. Easy visualization of the streamlines
3. Reduced velocity in water
4. Slower oscillation in water

All of these serve to facilitate observation of the flow phenomenon in the wind sensor, and an alteration of the model based on this observation may be incorporated in the air model with good insight to its effects.

It was hypothesized that the low frequency noise was the result of an instability of a vortex pair created by the interaction of the power jet and the fluid within the sensor. Figure 4a shows the wind sensor submerged in water flowing right to left at very low velocity. Note the pair of vortex rings near each receiver. Their slight shift toward the left is the result of the small free stream velocity in that direction. Figure 4b shows the effect of an increase in the free stream velocity. Note the disappearance of the vortex on the jet issuing in the same direction as the free stream flow. This is the result of the decrease in velocity gradient between the free stream and the power jet. The jet issuing against the free stream begins to oscillate, in what might be pictured as a cantilevered beam. This results in an oscillatory pressure recovered by the receiver. Further increase in velocity shows a periodic shedding of the vortex formed by the jet issuing into the wind (Figure 4c). This causes a noise at both receivers due to its gross alteration of the flow field.

Having isolated a major source of the noise, steps to reduce it were undertaken. Since the vortex pair was observed to oscillate when the free stream velocity was zero, it was thought that the instability of the stagnation plane of symmetry, located midway between the two receivers, was at fault. This low pressure region, from which both jets entrain fluid, was relieved by a circumferential slot in the flow straightening tube. Communication of this low pressure region with the stagnant surroundings was found to have no significant effect in reducing the noise. A second attempt to eliminate the low frequency noise was to break up the slowly shed vortices into smaller vortices. Although the smaller vortices are greater in number than the large, low frequency vortices, they decay more rapidly and are more easily filtered. Such higher frequency noise is often inherently filtered by instrument panel meters. The vortex breakup was accomplished by locating honeycomb in the vicinity of the power jets. This did reduce the noise and to a slight extent the gain ($\Delta P/\Delta V$) of the sensor, a

FLOW VISUALIZATION OF NOISE PHENOMENON

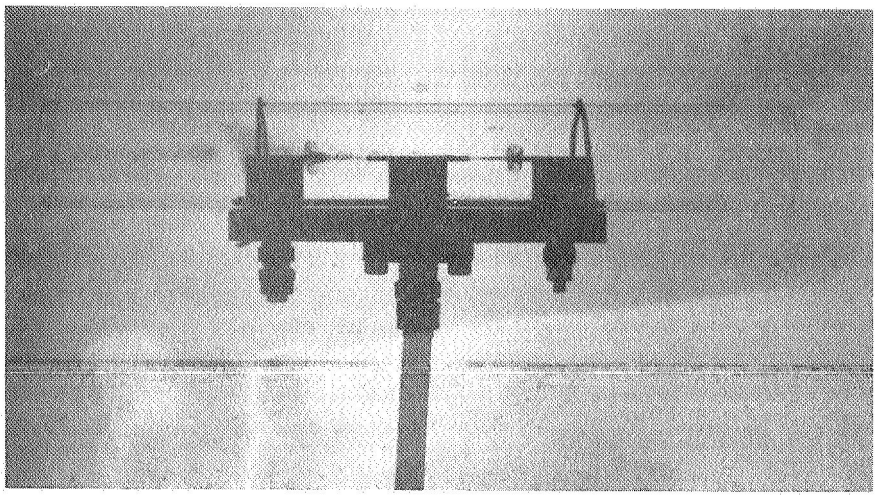

Figure 4a

$V \approx 0$

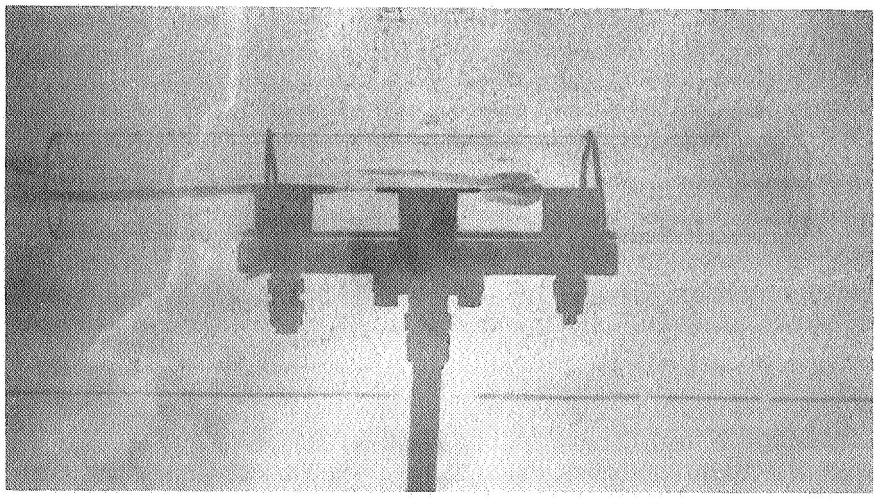

Figure 4b

INCREASED V

←

NOTE UPWARD DEFLECTION OF P_+ INTO STREAM

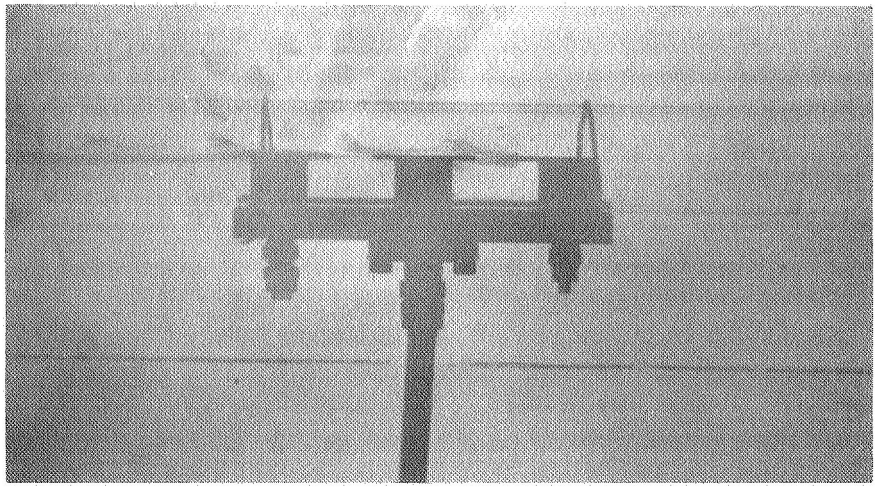

Figure 4c

FURTHER INCREASE IN V

←

NOTE SHED VORTICES

result which was anticipated from prior work (Reference 2). Employing this mechanism was found to introduce a more serious drawback. The ability to maintain a zero signal at zero wind velocity was lost. This null-instability is attributed to power jet attachment to and subsequent release from the honeycomb cells due to the well-known Coanda effect (Reference 8).

A final attempt to reduce the low frequency noise was internal contouring of the flow straightening tube to accelerate the flow and effectively increase the frequency of the oscillation. However, since the feature of sensor bidirectionality had to be maintained, contouring of the walls within the flow straightening tube had to be moderate to avoid flow separation. Should separation occur, the noise problem would be compounded due to its own unsteady nature.

An alternate approach was taken; make the effect of the noise less prominant. This was done by moving the receivers closer to the power nozzles and simultaneously increasing the receiver diameters. These have the effect of both decreasing "tip deflection" and having the full jet pressure persist at the receiver for a longer period of time during its oscillation. This has the general effect of also reducing the gain ($\Delta P/\Delta V$), but not so much that the S/N suffers for a fairly wide range of spacings.

Figure 5 shows the output differential pressure signal for a velocity of 17 ft/sec**. (This may be taken as an indication of gain.) The local maxima and minima do in fact exist, and are not to be construed as scatter in the data. Therefore, the spacing between power nozzle and receiver may be decreased from 0.45" to 0.43" or even to 0.41" without affecting the gain. Over this range of spacings (nominally 10%), the recovered total pressure at the receiver does not vary excessively. The spacing between local maxima and minima (nominally 0.020") indicates that the anomaly is traceable to the null adjust sleeve, which has 56 threads per inch.

Figure 6 shows the effect of an increase in receiver diameter. This results in a decrease in noise by a factor of approximately four. Tests with the aforementioned honeycomb to break up the vortices into high frequency and more rapidly dissipating vortices enabled a noise reduction of an order of magnitude. The simultaneous null instability, unfortunately, precludes the use of honeycomb for the time being.

**The maximum velocity in the low speed wind tunnel.

Figure 5.
EFFECT OF DISTANCE BETWEEN POWER NOZZLE EXIT AND RECEIVER

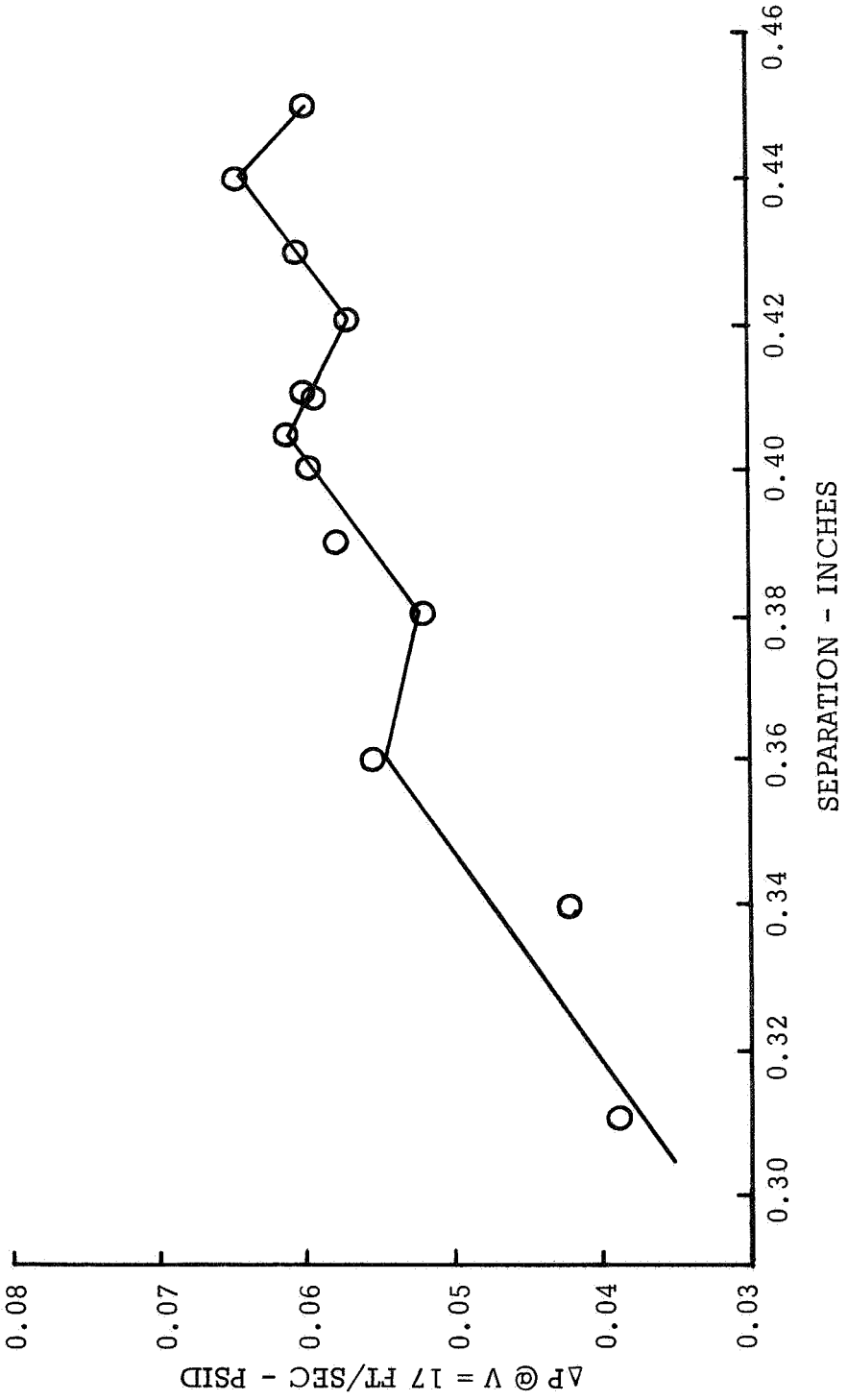

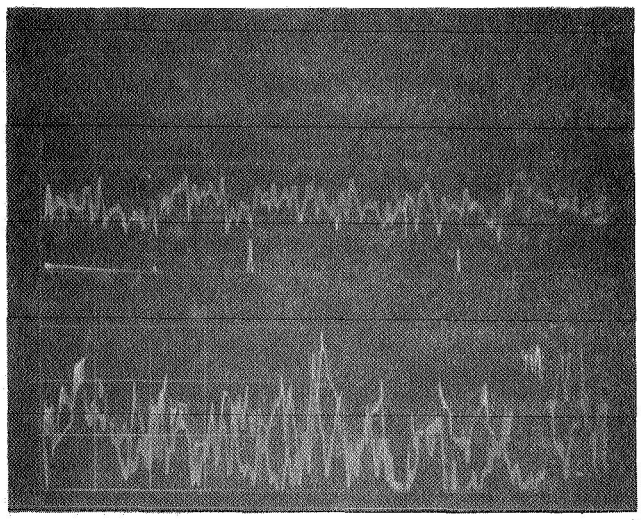

Figure 6.
COMPARISON OF THE NOISE WITH
TWO RECEIVER DIAMETERS

The flow visualization served to isolate the fluctuation in the flow field, and also provided a means of contending with it. While significantly reducing the noise, the basic simplicity of the concept was retained.

3.0 EXTERNAL CONFIGURATION

3.1 Angle of Attack Response

A second area of study was the external configuration of the wind sensor, as this has a direct bearing on the angle of attack -output signal characteristic. The early work on the sensor showed an angle of attack characteristic much like the well-known Kiel probe (Reference 9). The constant output up to 45^{o}, and particularly the anomaly for $70^{o} < \alpha < 90^{o}$ compound the difficulty of accurately obtaining total velocity vector information. For greatest simplicity in a multi-axis no moving part system, a cosine curve would be ideal. Two sensors mounted orthogonally would then measure the sine and cosine components of velocity, and these signals can be easily squared, summed, and square rooted for the total velocity. Simultaneously, the sine and cosine data provide the angle of the wind. This may be carried out by hand computation or through the use of standard electronic components. A no moving part three axis sensor can be similarly made.

Once again because of the complexity of the flow field, resort is made to flow visualization in order to determine the reason for the flow straightening tube actually counter-flowing the free stream for angles of attack in the range $70^{o} < \alpha < 90^{o}$, as seen in Figure 7. (Reproduced from Reference 2.)

In order to simplify the flow visualization still further for preliminary experiments, the flow straightening cylinder was idealized as a two dimensional channel configuration.

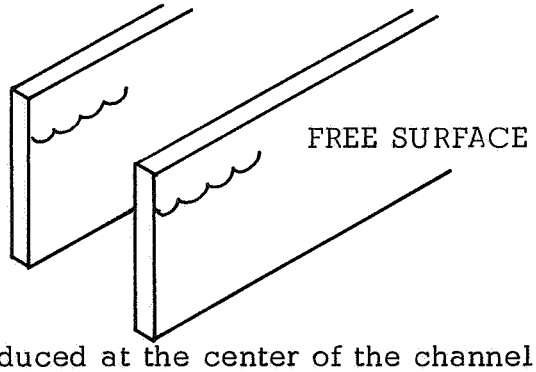

Dye is introduced at the center of the channel which is inclined 80^{o} to the free stream (the most severe angle from Figure 7). Observe that the dye exits through the upstream end, with the flow internal to the channel having a component opposite the free stream flow. This is the result of the free stream flow being deflected by the

BOWLES FLUIDICS CORPORATION
PARALLEL FLOW WIND SENSOR

OUTPUT PRESSURE

vs

ANGLE OF ATTACK

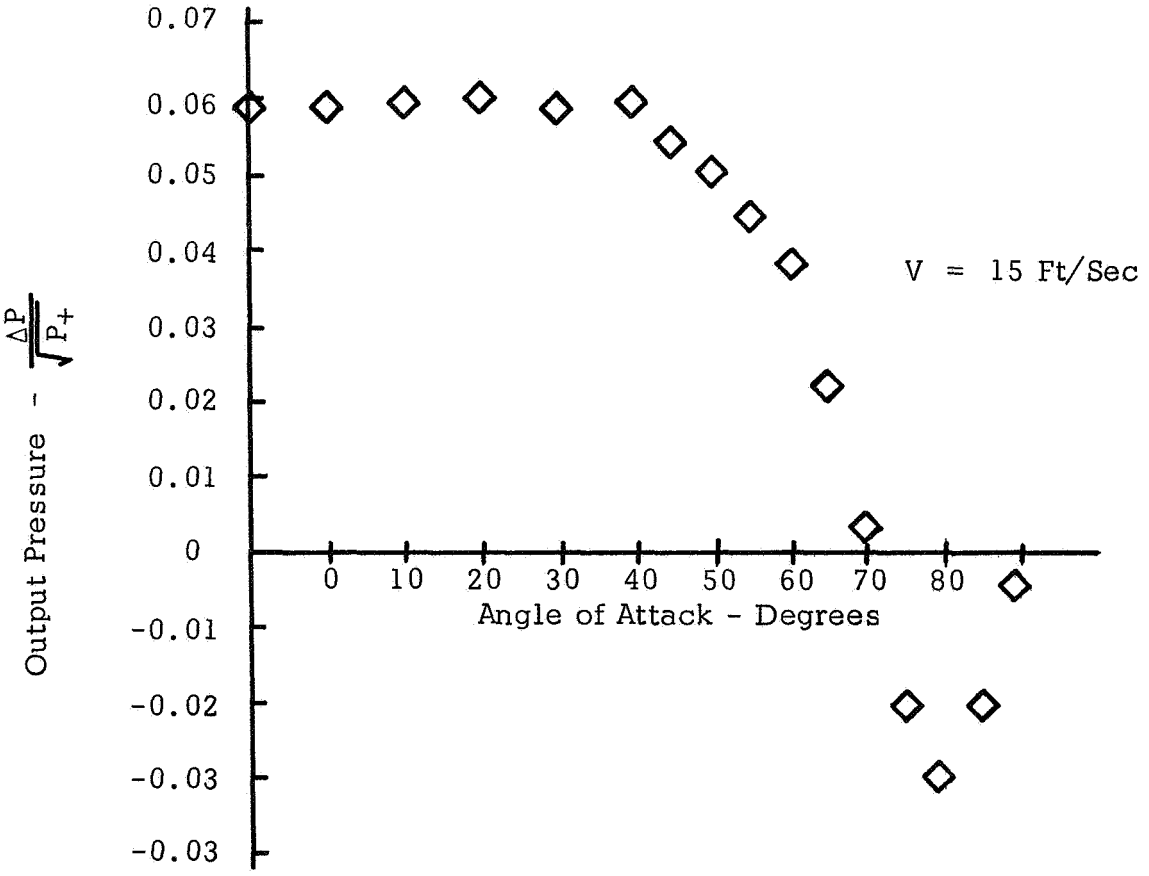

Figure 7.

presence of the flow straightening cylinder, and also the separation of the flow from it. A sketch of the phenomenon appears in Figure 8.

The streamline which is deflected and hence accelerated at point A causes a reduced static pressure. At the same time, the separation at point B causes a static pressure more nearly the total pressure of the free stream. The net result is a differential pressure across the channel and a flow through it with a component opposite to that of the free stream. For angles greater than 80°, the deflection at A and the separation at point B are not as severe and the pressure gradient across the length of the tube decreases. The "negative" flow through the sensor diminishes to zero at 90°. A well rounded entrance was next tested, and this produced the desired result that the internal flow exits with a component in the same direction as the free stream (Figure 9). This was used as the starting point for a series of wind tunnel tests of toroidal (derived from the 2-dimensional cylindrical) end sections to determine the minimum feasible size. Figure 10 shows the effect of toroid-to-flow straightening cylinder ratios of 0, 0.4, 0.8. These inlets tend to exhibit a slightly increasing output signal for $\alpha < 40^{\circ}$. Most important, is the information that for $d/D > 0.4$, the counterflow through the flow straightening cylinder disappears.

A second entrance configuration was then wind tunnel tested. This was a diffuser which provided a relatively small frontal area and boat-tailed afterbody, thereby reducing the separation which is considered to be a source of the difficulty for $70^{\circ} < \alpha < 90^{\circ}$. This entrance did a great deal to reduce the angular response problem, but did not entirely eliminate it; moreover, through continuity of mass flow through the cylinder it reduced the effective free stream velocity over the power jets, which in turn reduced the gain of the sensor. This can be seen by comparing Figures 10 and 11 which were measured at the same velocity. Because of the drastic reduction in gain, no further testing on this type of inlet took place.

The last approach to solving the angle of attack problem was fashioned after the "split flap" concept used to prevent flow separation on aircraft (Reference 10). An annular gap was created between the original flow straightening cylinder and a short cylindrical length (Figure 12). The purpose of this gap is to reduce the flow separation at one end of the flow straightening cylinder and the deflection of the free stream at the other. These short sections were tested at various distances from the edge of the flow straightening cylinder, and while this configuration offers no advantage over $70^{\circ} < \alpha < 90^{\circ}$, it appears to provide

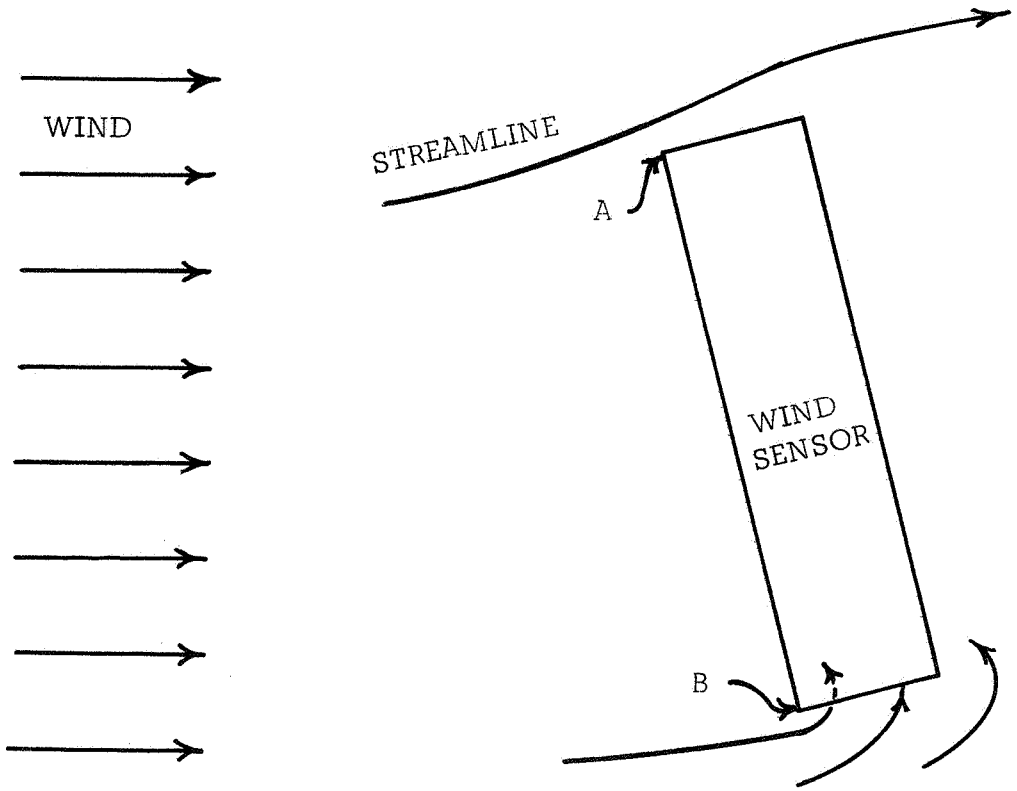

Figure 8.
FLOW PATTERN AT SEVERE ANGLE OF ATTACK

Figure 9.
FLOW VISUALIZATION OF ANGLE OF ATTACK PHENOMENON

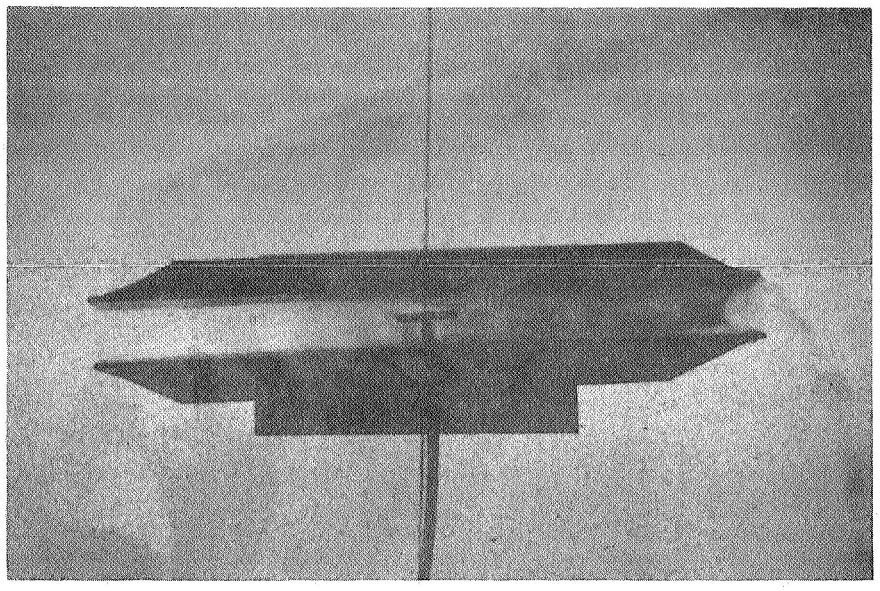

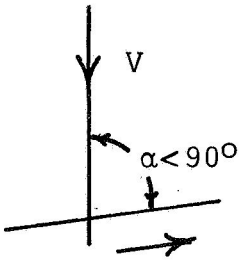

VELOCITY
COMPONENT
IN SENSOR

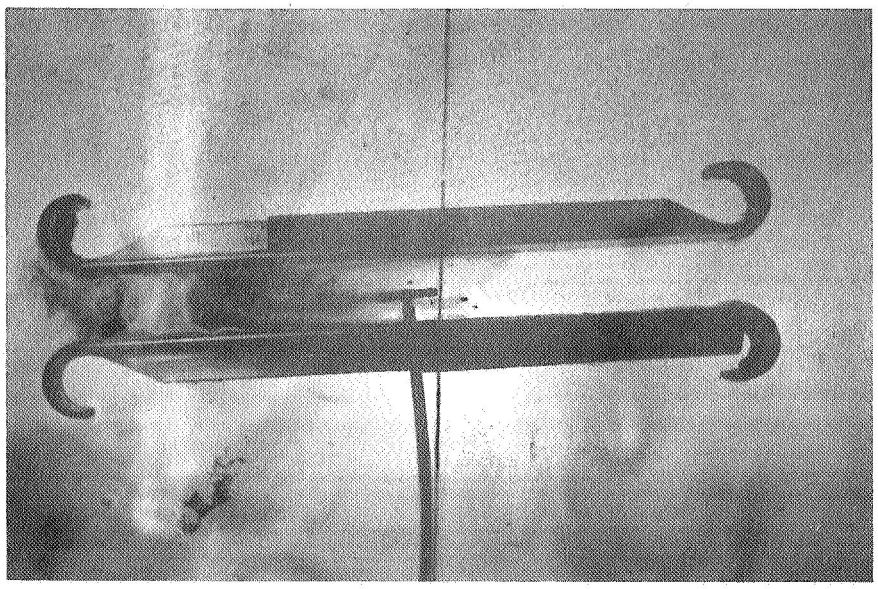

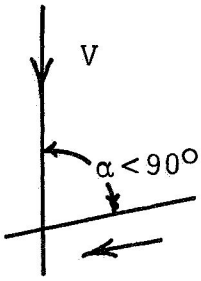

VELOCITY
COMPONENT
IN SENSOR

Figure 10.
OUTPUT PRESSURE VS ANGLE OF ATTACK, TOROIDAL ENTRANCE

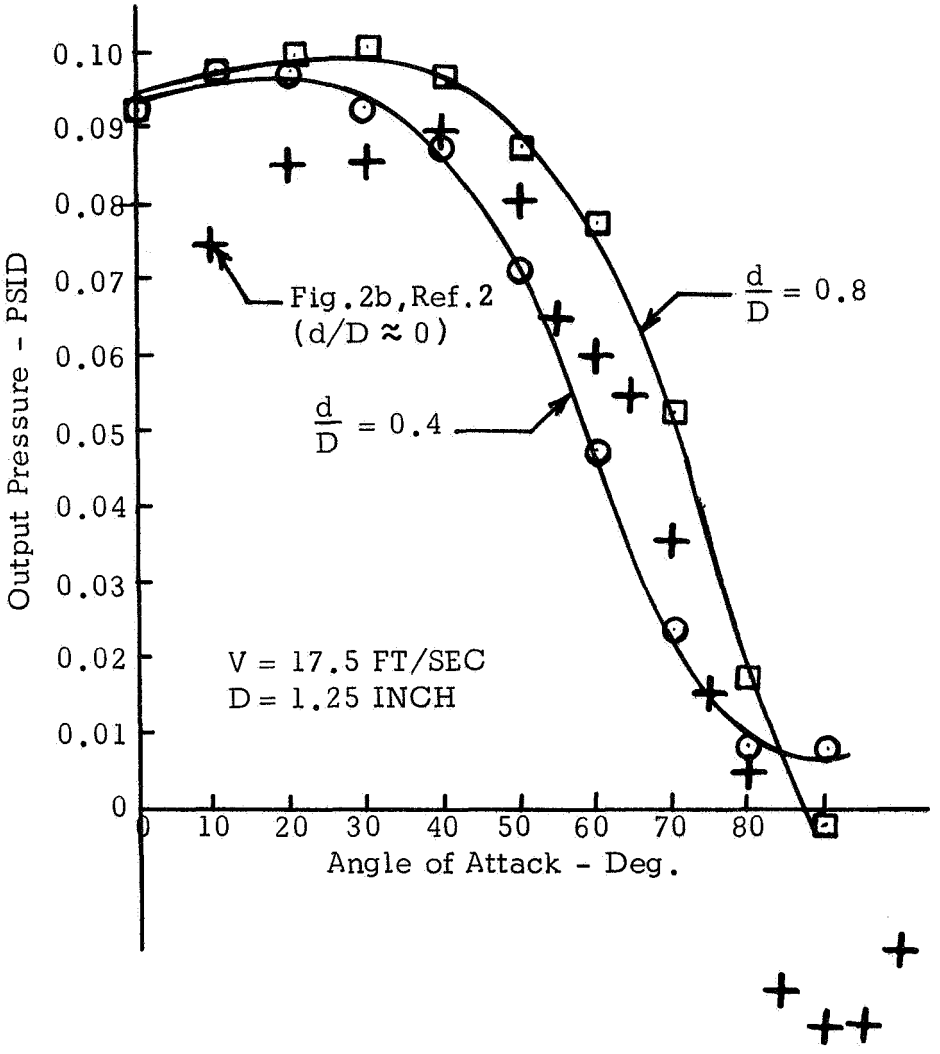

Figure 11.
OUTPUT PRESSURE VS ANGLE OF ATTACK, DIFFUSER ENTRANCE

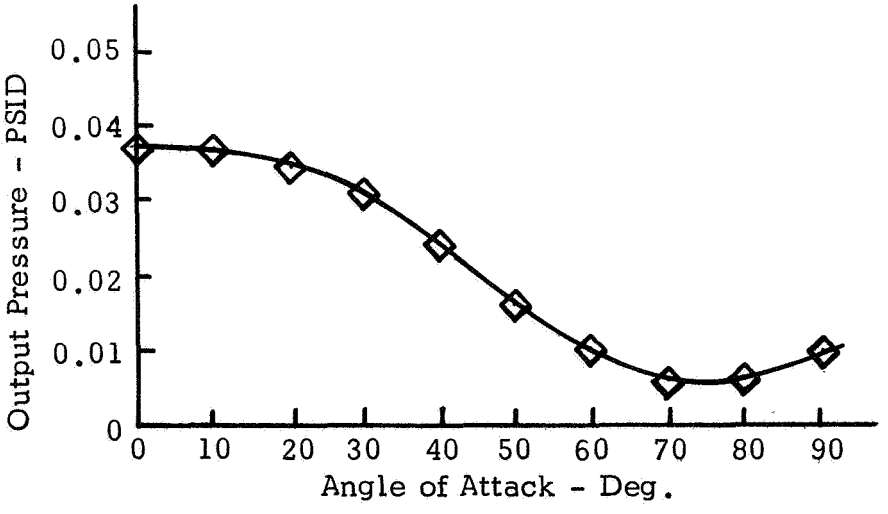

Figure 12.
OUTPUT PRESSURE VS ANGLE OF ATTACK,
SPLIT FLAP CONCEPT

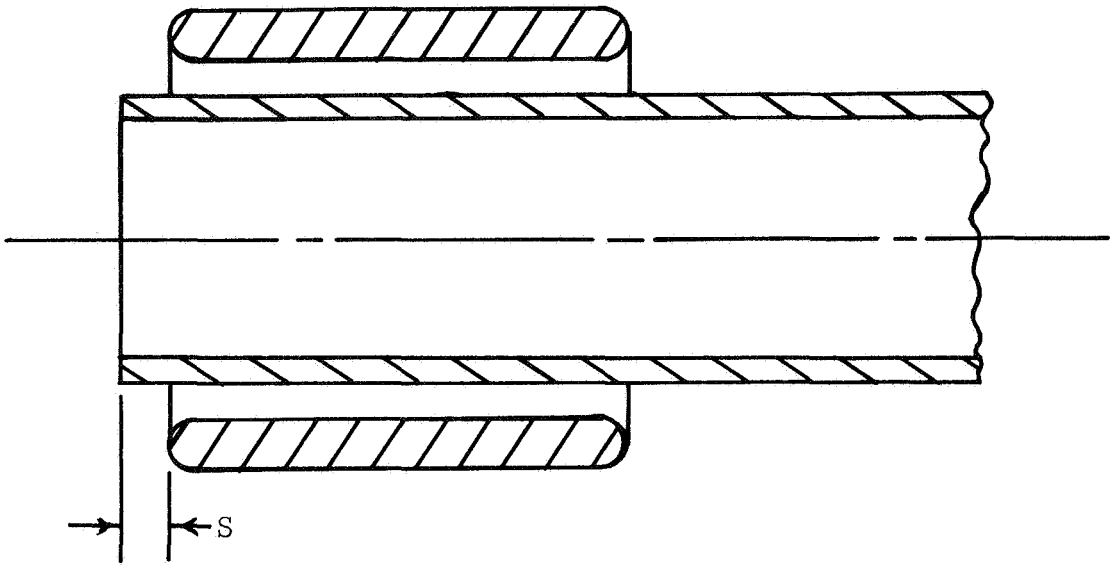

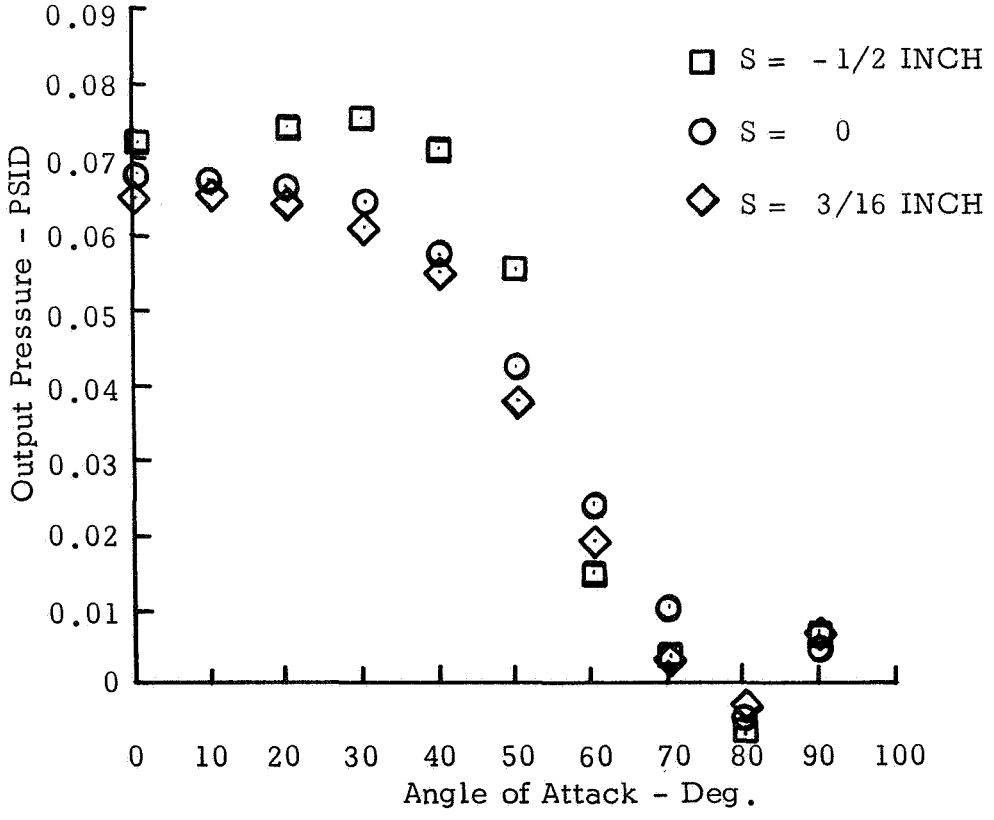

a better approximation to the cosine curve at lower angle of attack by the output pressure decreasing at small angles rather than holding flat as was shown in Figure 7.

In general, it may be concluded that considerably more work can be done to provide a cosine variation of output pressure with the sensor's angle of inclination to the approaching flow. Because the primary objective of this program is to develop a single axis sensor, further work in this area was considered unwarranted at this time.

The unit as it stands can be fitted with end pieces to quite accurately (less than 10%) resolve angles with available electronic computational modules. Without this advance, where a characteristic such as shown in Figure 7 existed, angular resolving from a practical sense would have been impossible.

3.2 Effect of Wind Sensor Size

Anticipating a flight test model, it is of interest to reduce the size of the sensor. The power nozzle diameter cannot be appreciably reduced, for then there exists the possibility of the power jets being laminar. If that were to occur, the phenomenon of transition from the laminar to the turbulent flow regime would also occur. Because the transition of the jets could not take place simultaneously, an extraneous and unpredictable output differential pressure would result.

The flow straightening cylinder can be shortened with no detectable change in performance. The diameter of the flow straightening cylinder was reduced with the effect shown in Figure 13. As the diameter decreases, the power jet flow fills the cylinder and rapidly creates a choking effect for the free stream, which is supposed to pass through uninhibited. Decreasing the diameter has the effect of raising the threshold velocity. Here is an instance where size and threshold must be traded off with a particular application in mind.

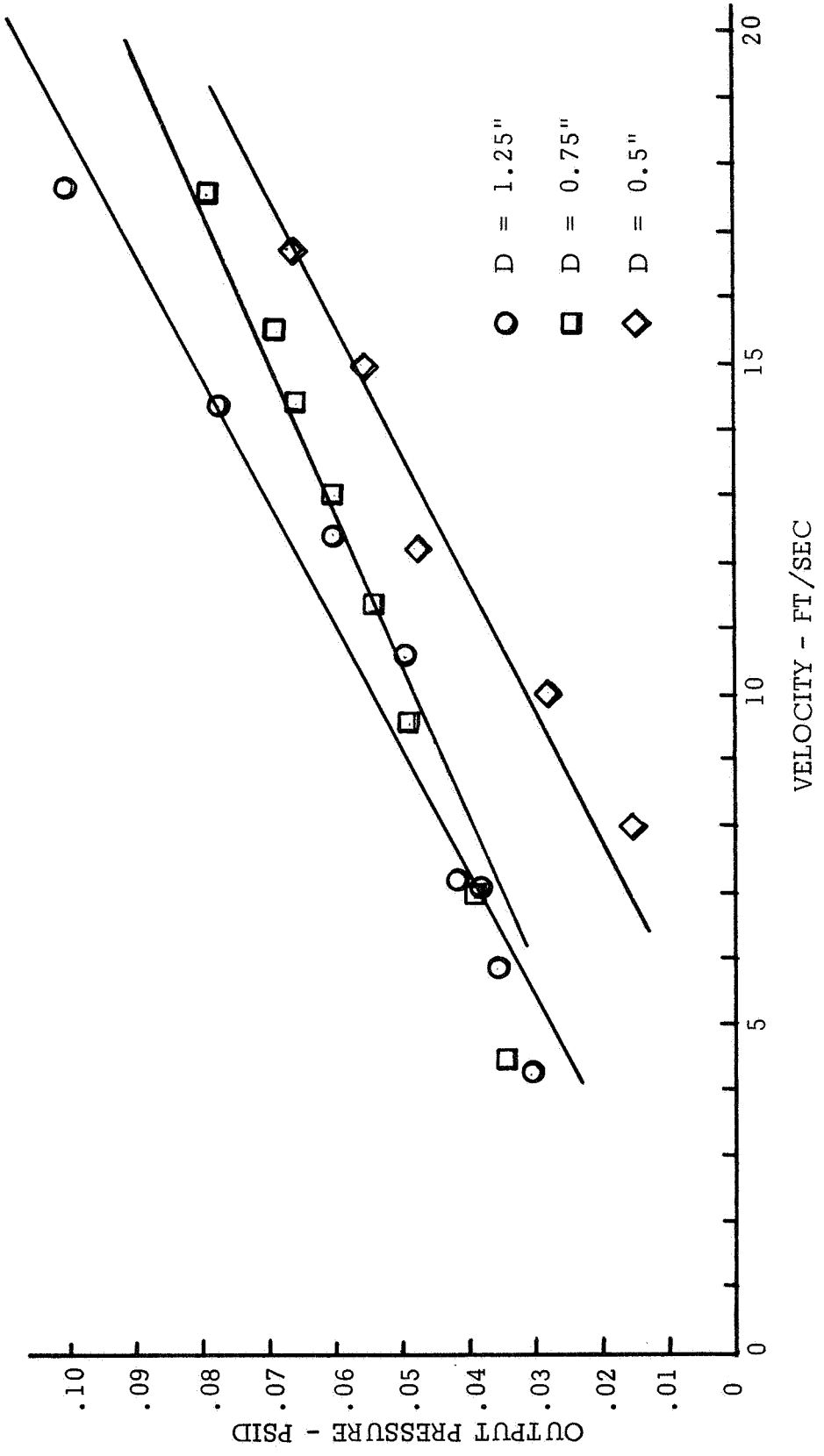

Figure 13.
EFFECT OF FLOW STRAIGHTENING CYLINDER

4.0 FLIGHT TEST MODEL DESIGN

The major effort of this program is to design and fabricate a flight-worthy single axis sensor based on the research conducted in the areas of signal noise and angular response. The sensor, complete with monitoring instrumentation and deicing means is to be delivered at the conclusion of the program.

4.1 Monitoring Instrumentation

The instrumentation package consists of a pressure regulator, differential pressure transducers, amplifier, low pass filter and batteries. A filter has been included to simulate the damping which a panel meter would provide, since much of the noise is the characteristic high frequency of jet noise. Figure 14a shows a schematic of the complete instrumentation package. In the package are two temperature compensated differential pressure transducers. The schematic for the dc exitation transducer bridge circuitry is shown in Figure 14b. One transducer has a range of 10 psid and a full scale output of 40 mv. This is used to measure the supply pressure which is simultaneously displayed on the 0 - 5 psid pressure gage. The instrument package appears in Figure 14c. The wind sensor is operated at a designated set point, such as 4.5 psi on the gage. This corresponds to a supply jet total pressure of 3.0. Because of the losses in the manifolding which supplies the sensor nozzles, operating pressure and the jet total pressure are not equal. They are, however, related through Figure 15.

The second transducer is $\pm$ 1 psid, and its corresponding voltage is $\pm$ 30 mv. Because of the low output pressure signal levels at low velocity and consequently low voltage levels, this transducer is connected to an instrumentation amplifier (Burr-Brown Model 1632A) which has fixed gains of 1, 10, and 100. This amplifier and the filter have provision for balancing out their own zero signal offset. This has been adjusted prior to shipping, and should require no further attention.

It is considered worthwhile to incorporate an active low pass filter (Burr-Brown Model 5703-LP4B-2R00) in order to attenuate high frequency noise of the system.

As shown in the schematic (Figure 14a), the pressure regulates to maintain a constant differential pressure between the supply and the local ambient, regardless of the value of the latter. In this

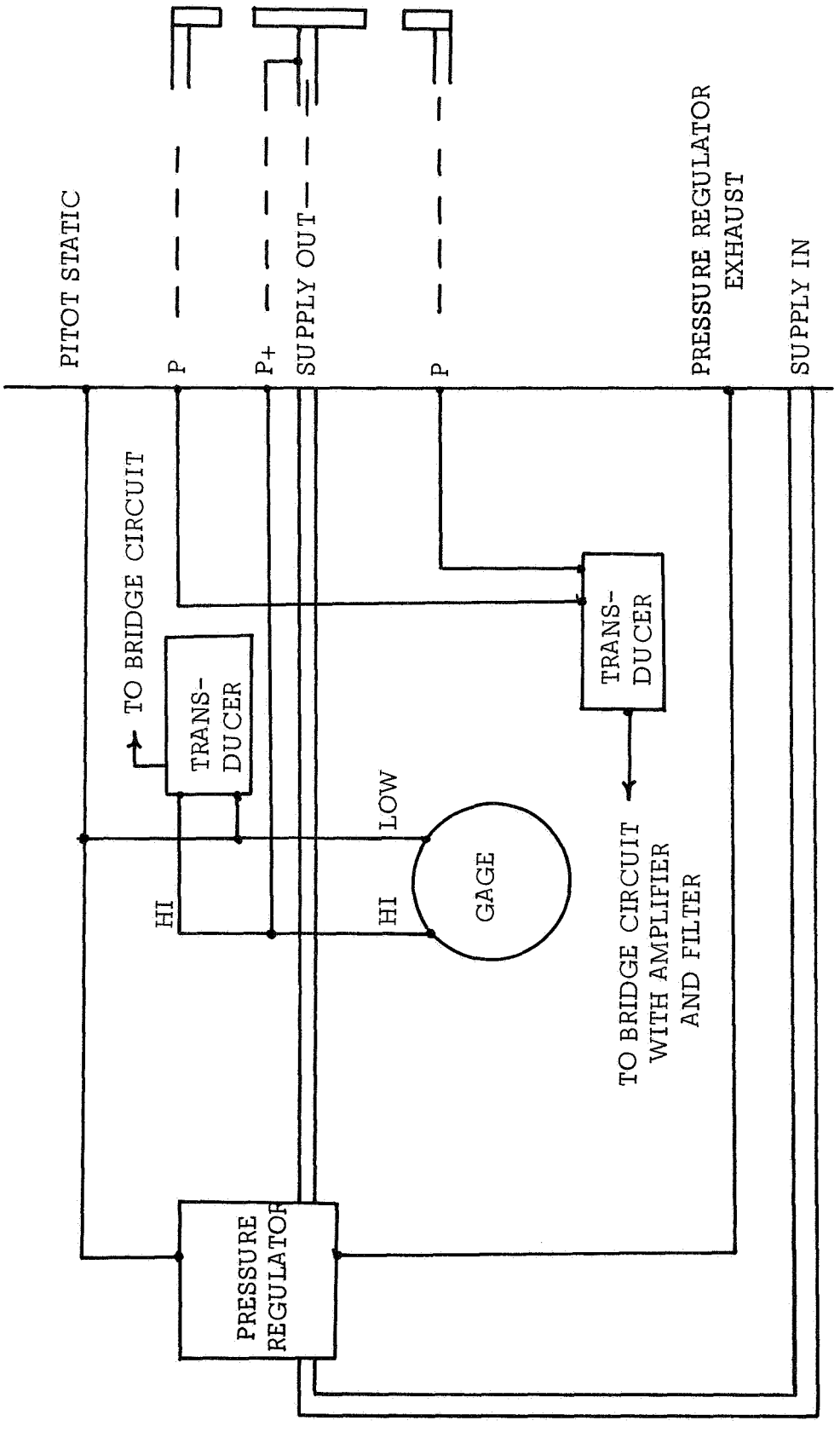

Figure 14a.
SCHEMATIC FOR WIND SENSOR INSTRUMENTATION PACKAGE

Figure 14b.
SCHEMATIC OF ELECTRICAL CIRCUITRY IN INSTRUMENTATION

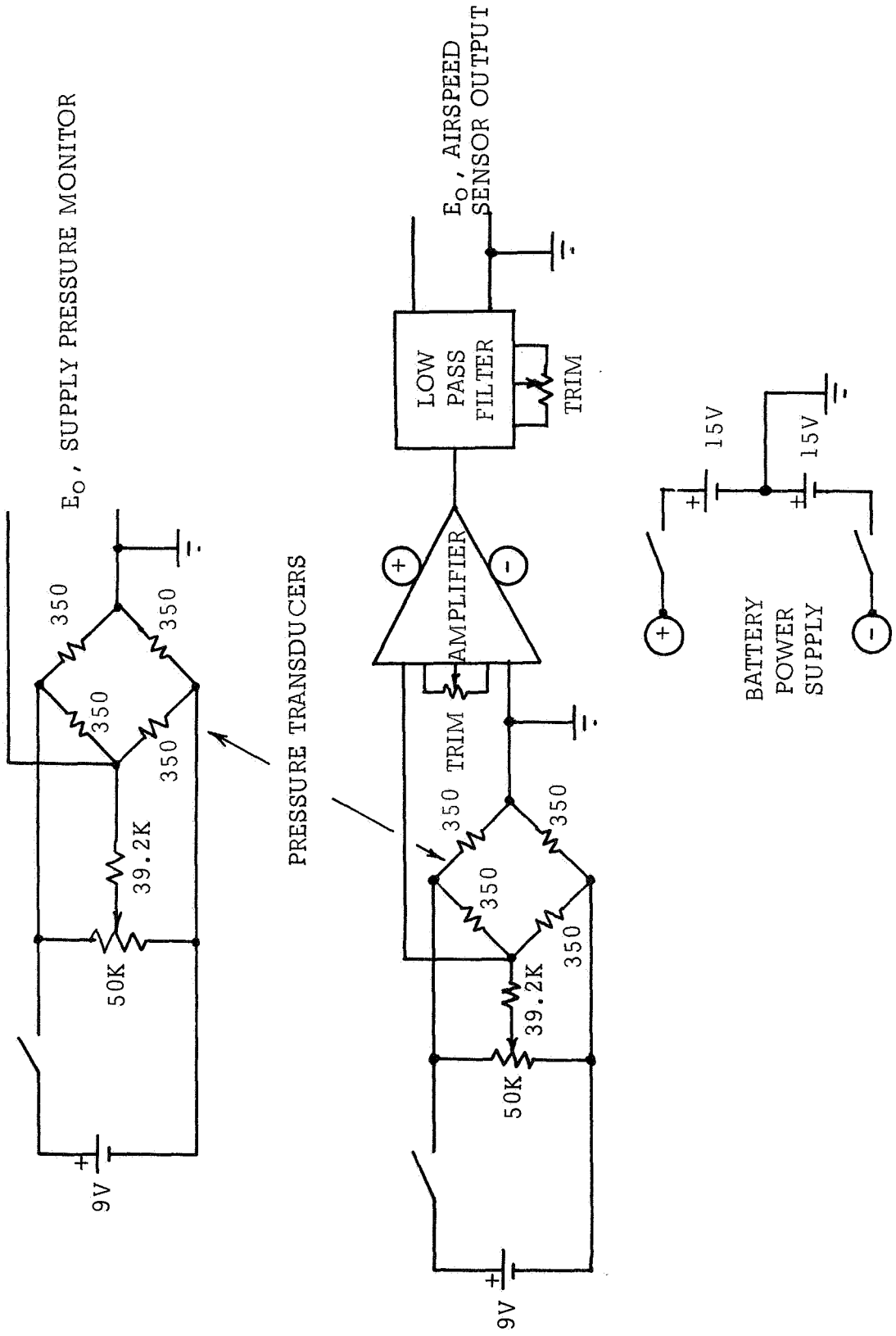

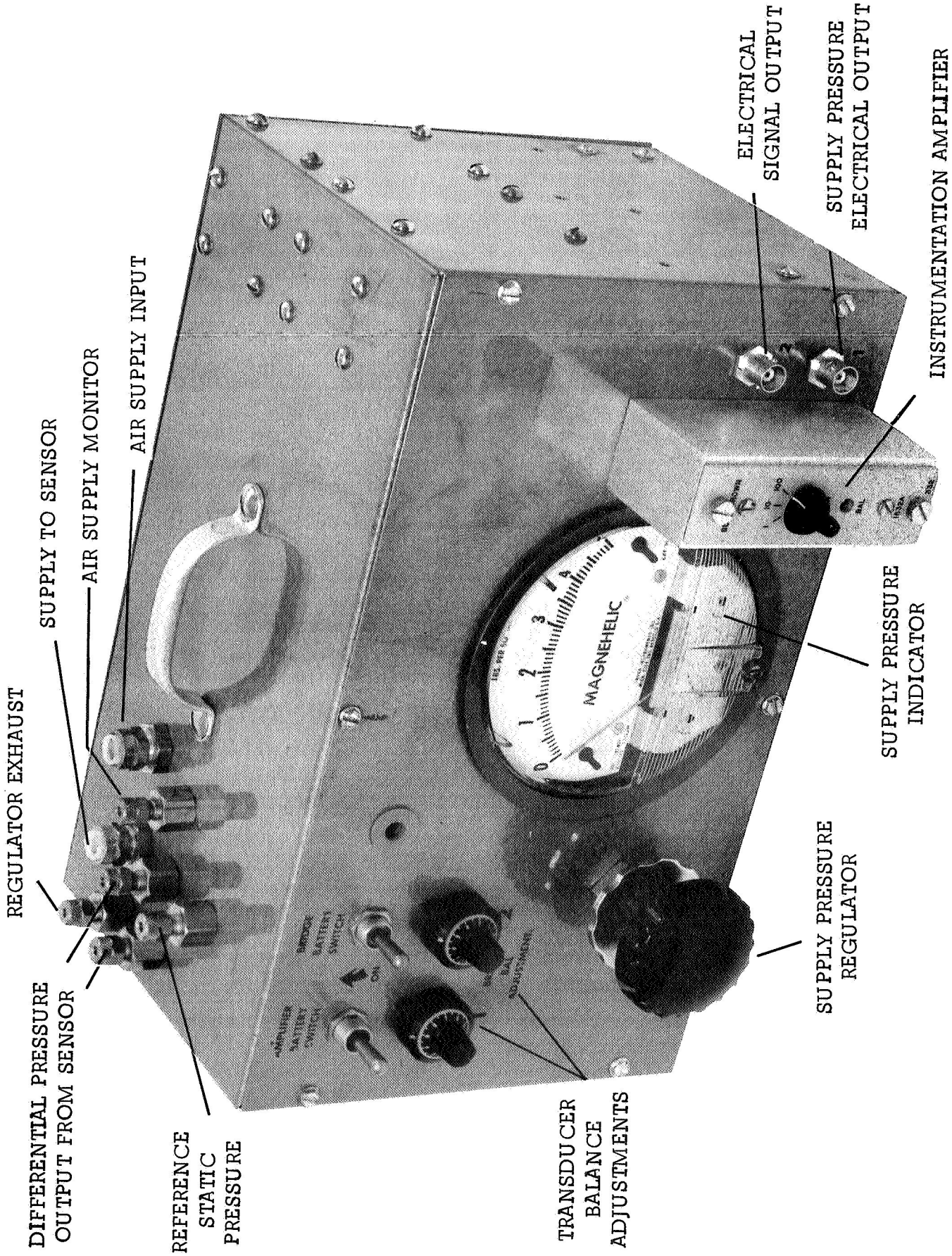

Figure 14c. PHOTOGRAPH OF INSTRUMENTATION PACKAGE

Figure 15.
JET TOTAL PRESSURE AND FLOW
RATE VS GAGE PRESSURE READING

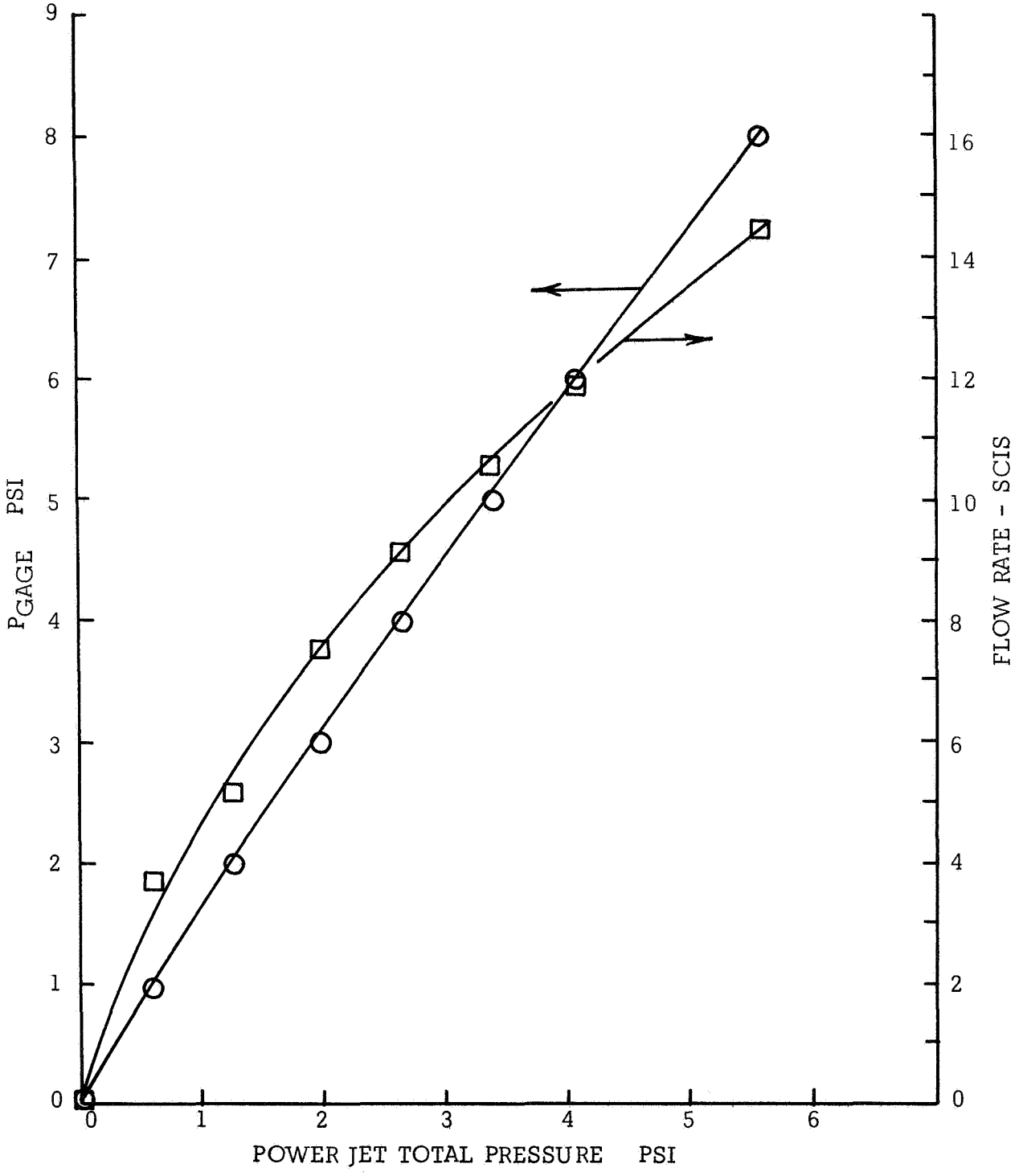

way, effects of change in altitude are minimized, for a reduction in density (associated with increase in altitude) is accompanied with an increase of power jet velocity. This increases the gain of the sensor (Reference 2, Figure 4), and it is felt that the result gives a fairly accurate measure of true air speed. The exhaust port of the regulator is also fed to the ambient, and this is a part of the feedback system of the regulator itself. It is anticipated that the local pressure reference will be the static pressure port of a pitot tube for flight testing. The flow through the lines marked pitot static and exhaust in Figure 14 will affect the static pressure readings only in the transient state. Moreover, since the rate of climb or descent of aircraft is not severe, the effect is considered to be minimal.

4.2 Fluidic Wind Sensor

The Fluidic wind sensor itself which is built according to Mil Specs (References 11, 12), is provided with null adjust and deicing means, and is intended for boom mounting. The dimensions of the adaptor to the boom are shown in Figure 16.

The completed unit is shown in Figures 17a and 17b. The toroidal end caps of diameter ratio $d/D = 0.6$ was chosen as a compromise between ideal angular response and size considerations (see Figure 10). The choice was influenced by the fact that this particular sensor is specifically for single axis testing. Figure 17b shows the simple means of null adjustment. A threaded sleeve on the centerline of the receiver allows varying the distance of power nozzle to receiver. No lateral motion of the receiver is necessary due to the receiver being larger than the power nozzle.

The deicer is designed specifically for the sensor shown in Figure 17. The unit has a 200 watt-80 volt maximum capacity.

Applying the designated value of 80 volts to the finished deicer showed that there is insufficient heat conducted to the nozzle assembly to absolutely insure deicing in severe cases. This can be remedied to a great extent through the use of a single material of fabrication throughout. Also evident after preliminary testing is the fact that the pedestal is a good heat sink, and therefore should be insulated from the flow straightening cylinder. In future models this can easily be accomplished by relieving the cradle portion of the pedestal to reduce contact area.

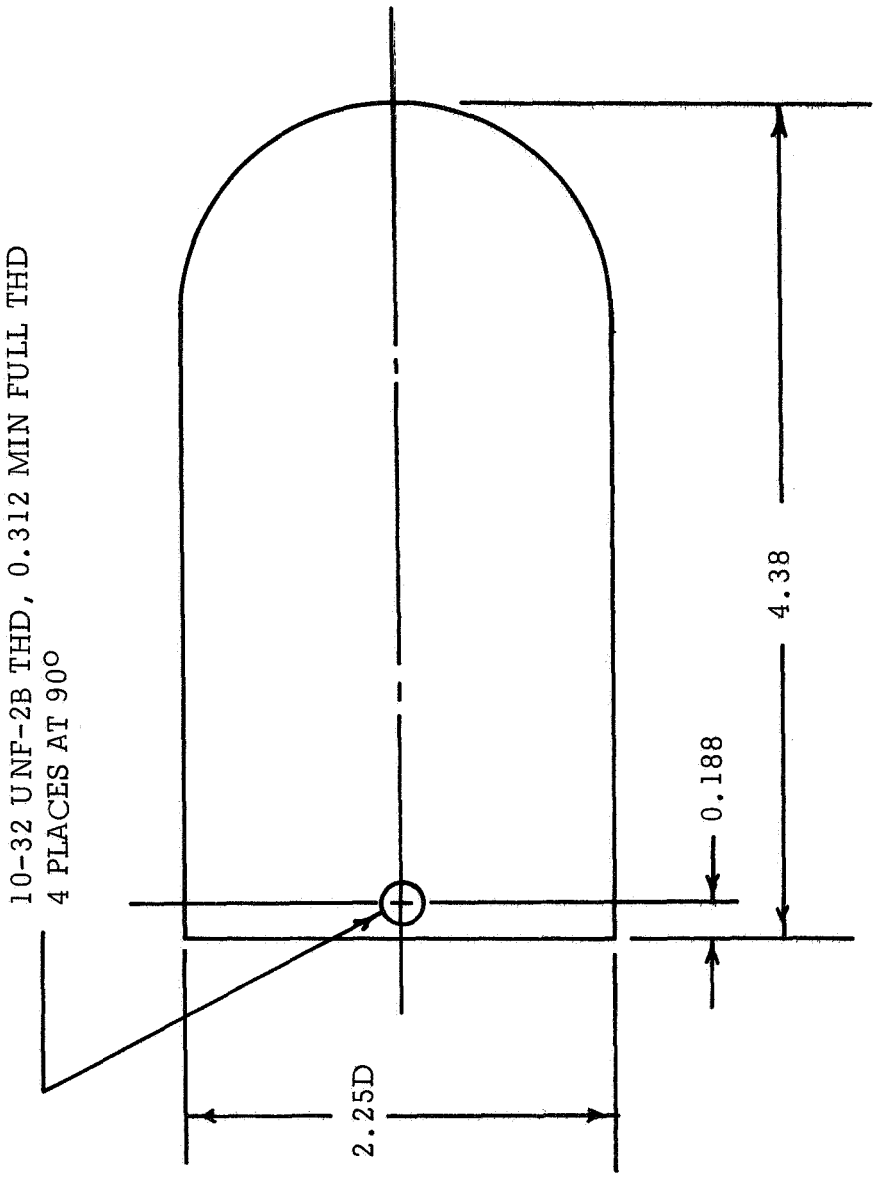

Figure 16.
BOOM ADAPTOR

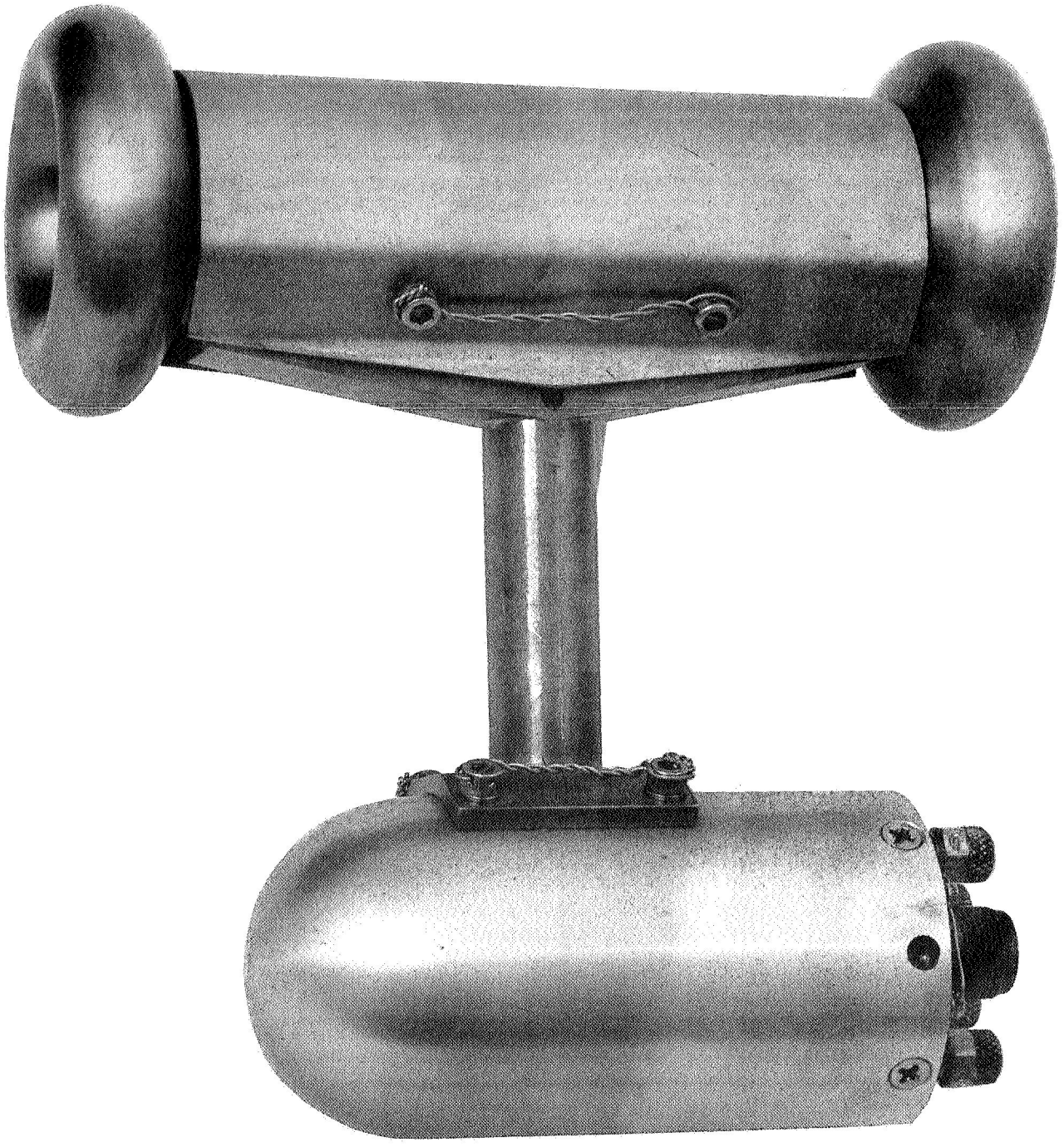

Figure 17a. ASSEMBLED WIND SENSOR PHOTOGRAPH

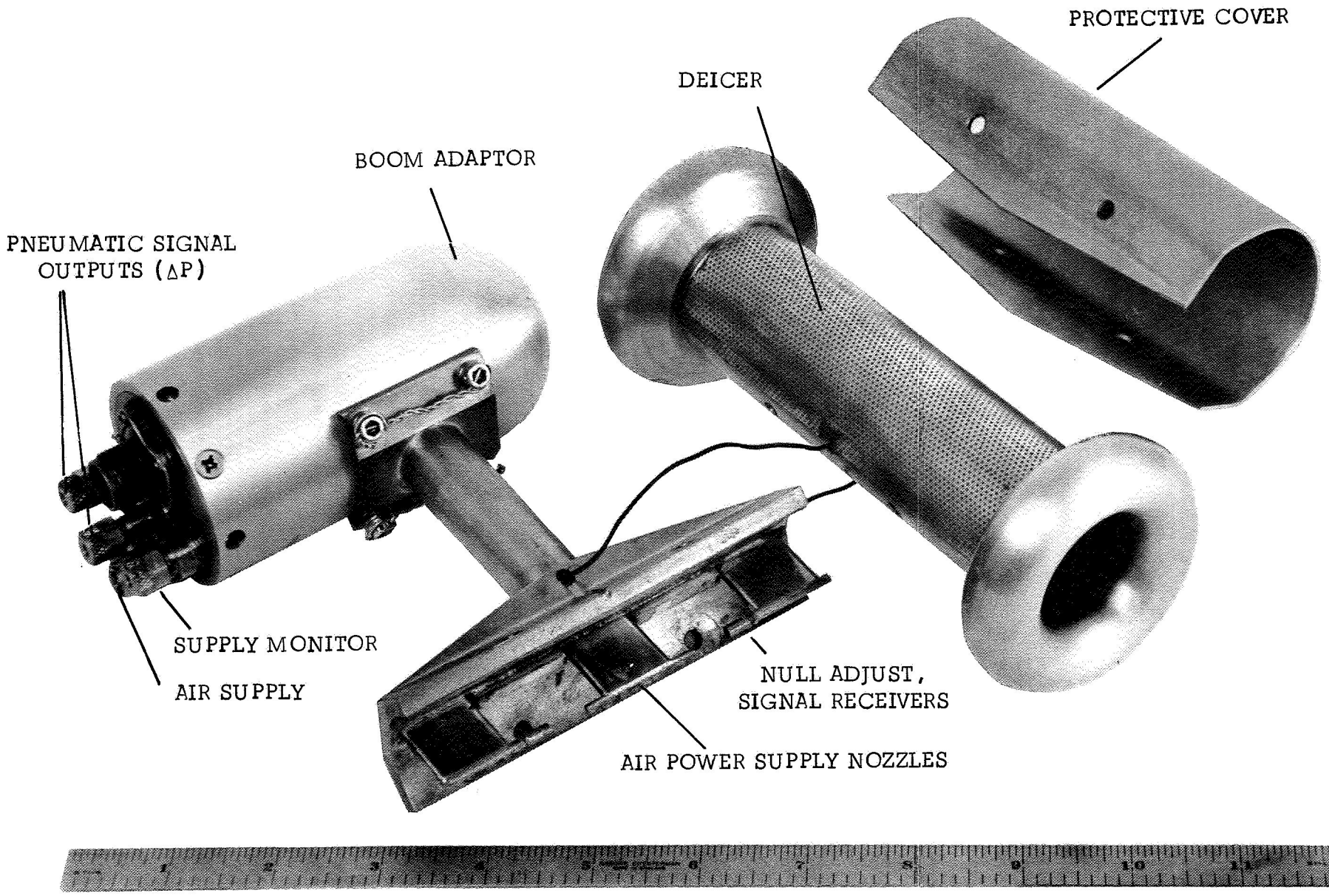

Figure 17b. DISASSEMBLED WIND SENSOR PHOTOGRAPH

5.0 WIND TUNNEL CALIBRATION OF THE SENSOR

Low speed wind tunnel testing was carried out at Bowles Fluidics Corporation where the specially designed tunnel built under contract NAS 12-2038 (Reference 2) is located. For the higher speeds, the low speed tunnel at the University of Maryland was used. The maximum velocity of the BFC tunnel and the minimum velocity of the University of Maryland tunnel overlapped, and correlation of the results in the two tunnels were excellent. Tests were conducted at three supply pressures, each measured relative to the wind tunnel ambient static pressure (which is less than atmosphere). The sensor was tested over the range $-160 \leq V \leq 160$ ft/sec. At several values of velocity, the angle of attack characteristic was obtained over the complete 360^{o} range. The unit was then rotated 90^{o} about the flow straightening cylinder centerline, and once again tested over the angle of attack range of $0\text{-}360^{o}$ to verify its ability to resolve angles.

The calibration curve of ΔP vs V is shown for each of the supply pressures (power jet total pressures) in Figures 18, 19 and 20. As is characteristic of the sensor, the data are quasi-linear over the entire range, and better linearity is achieved at higher supply pressures. Most significant is the symmetry about the origin and the finite slope of the curve at zero velocity. Figure 21 shows the low speed portion of Figure 19. Note that in the range $-20 < V < 20$ ft/sec the sensor is quite linear. Figure 22 is the data normalized by P_+. (Note that P_+ is proportional to power jet velocity, and that the principle of operation of the sensor is viscous shear which is dependent on difference in velocity in two laminas of fluid.) Finally, Figure 23 is representative of the angular response of the sensor. Less error could be achieved by using larger toroidal end caps or a combination of two or more of the other end caps previously discussed. The supply pressures shown on the graphs are the actual jet total pressure measured on the jet centerline a few power nozzle width from the nozzle exit.

Figure 18.
DIFFERENTIAL OUTPUT PRESSURE VS VELOCITY

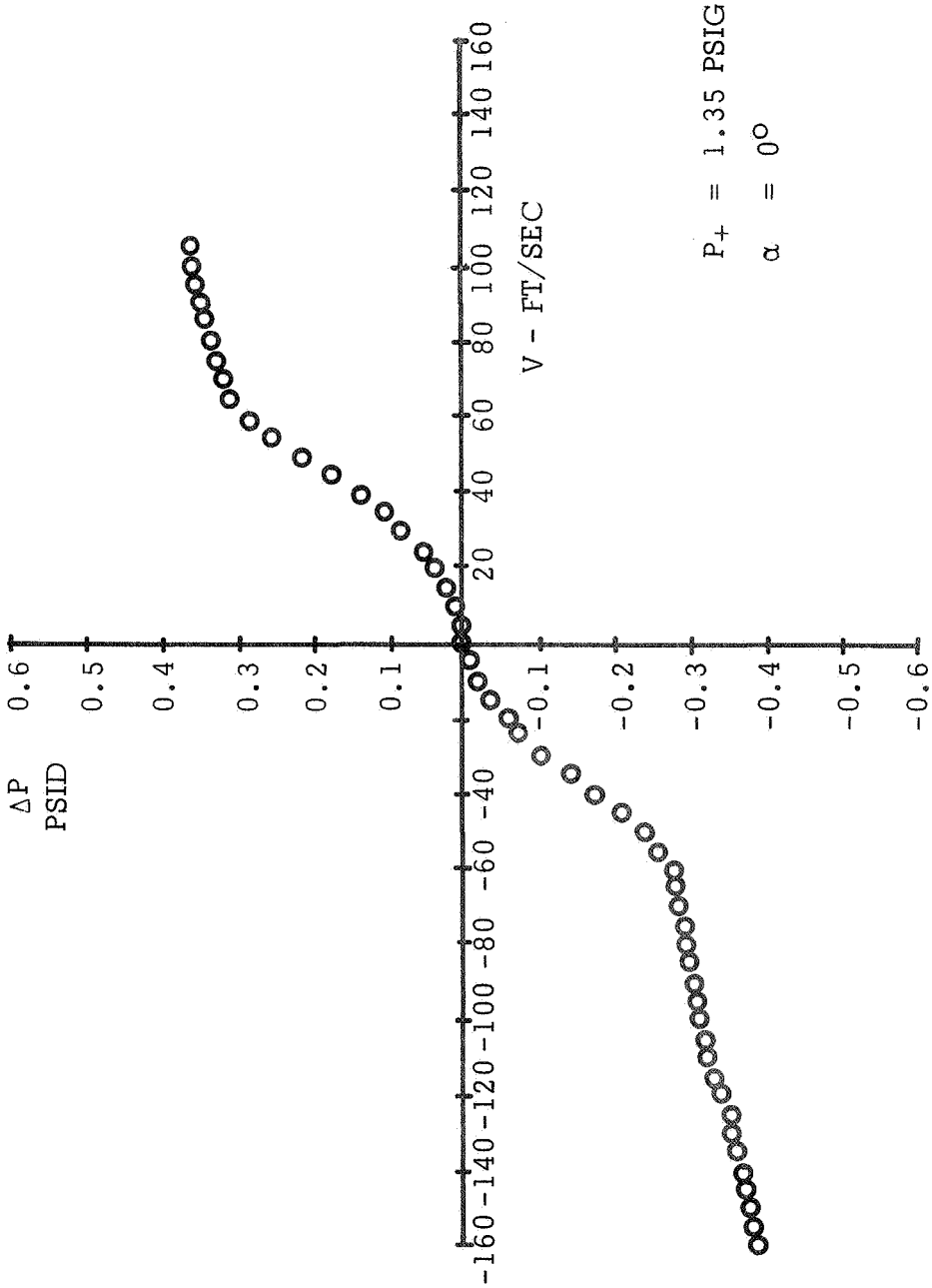

31664

Figure 19.
DIFFERENTIAL OUTPUT PRESSURE VS VELOCITY

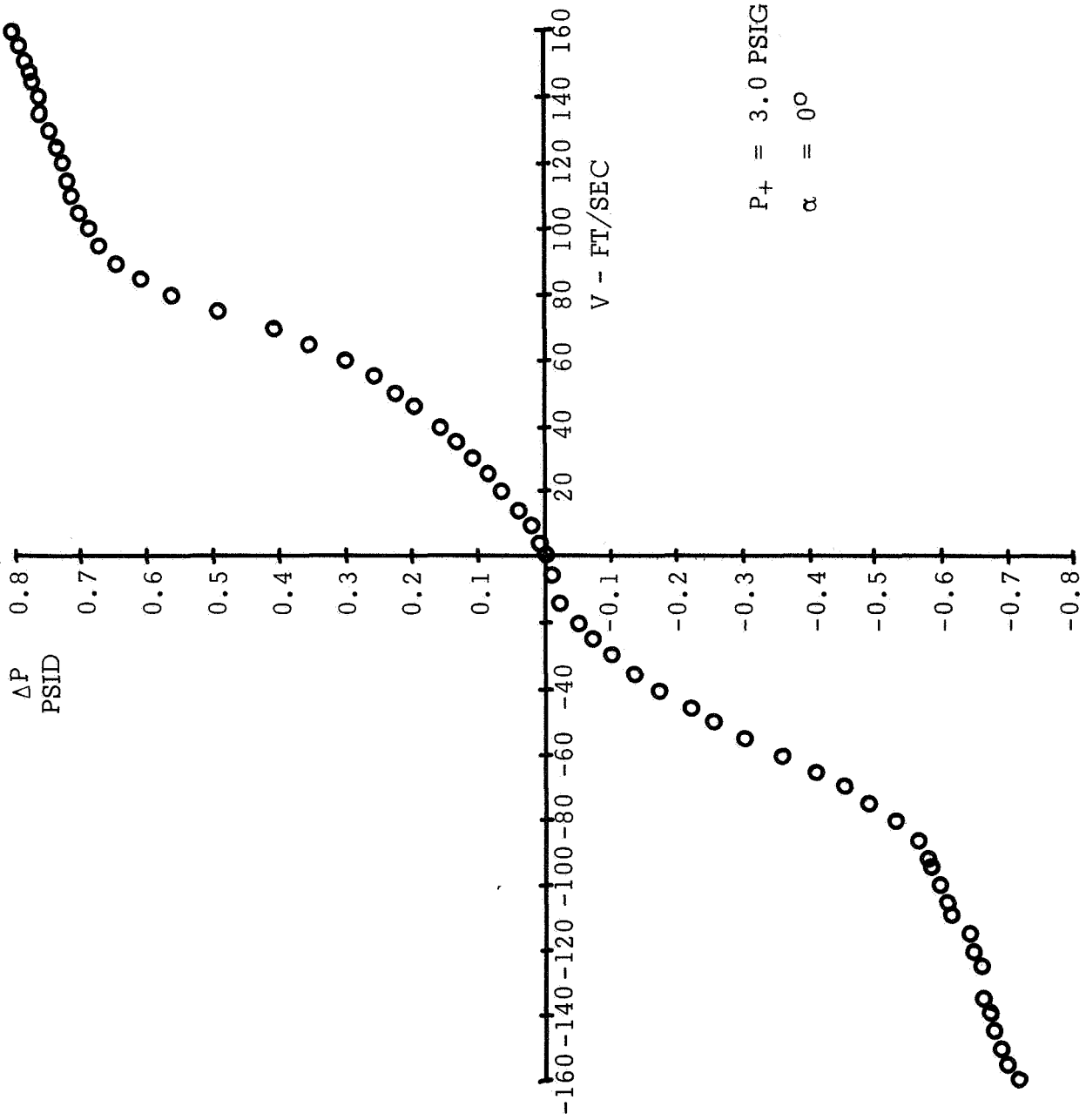

Figure 20.
DIFFERENTIAL OUTPUT PRESSURE VS VELOCITY

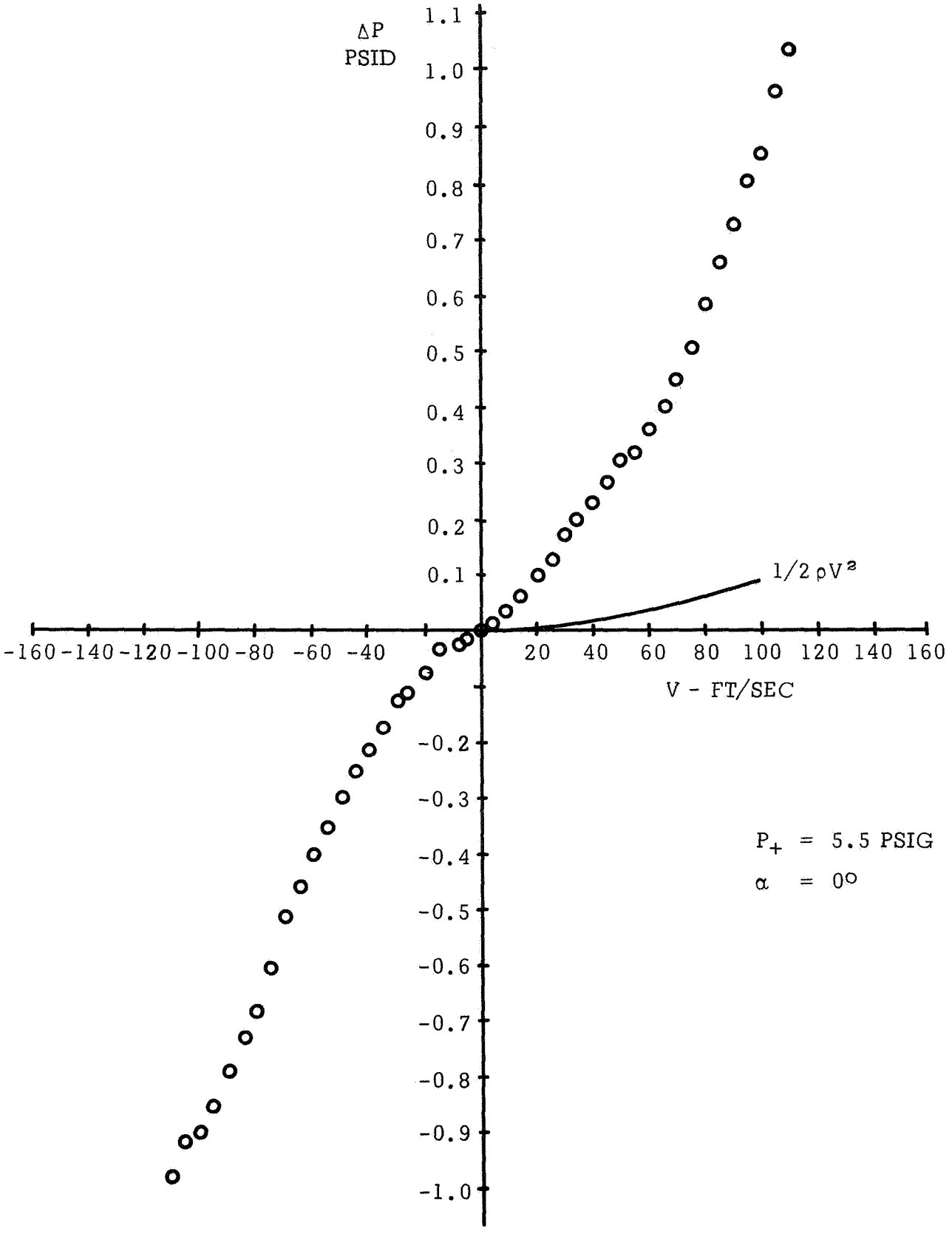

Figure 21.
LOW SPEED OUTPUT PRESSURE VS VELOCITY

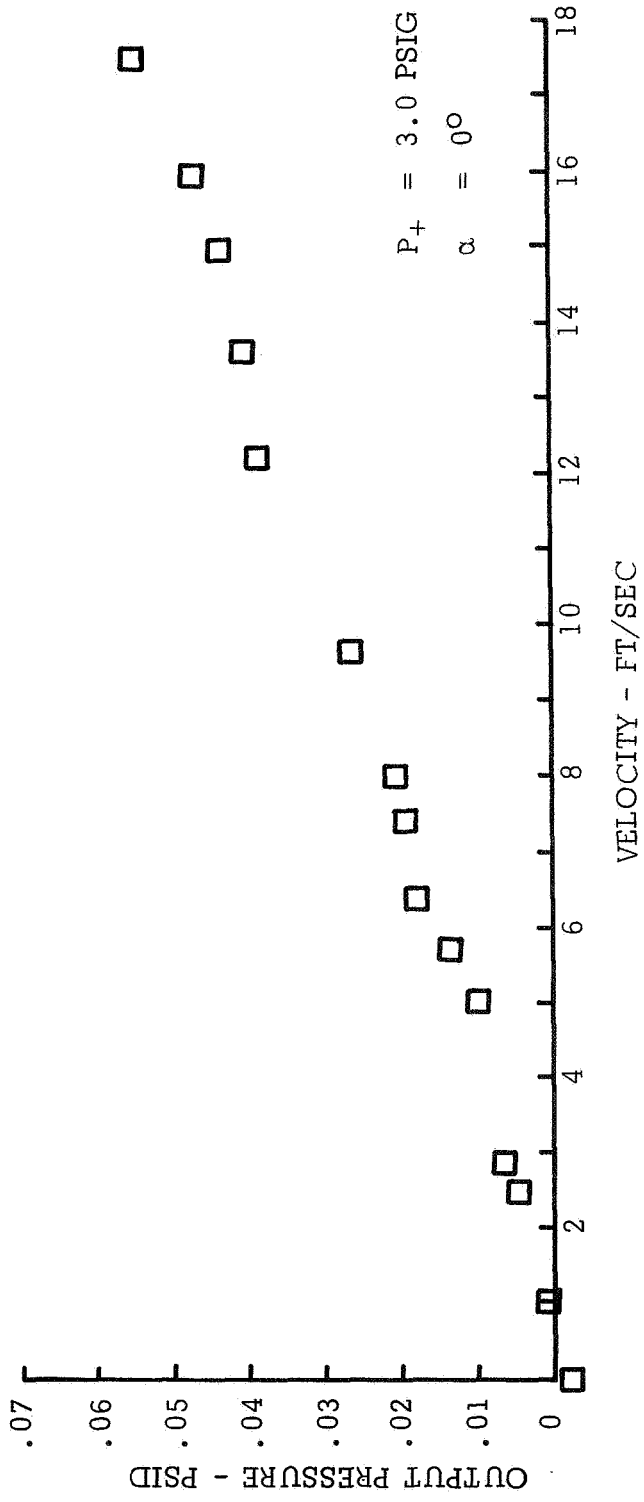

Figure 22.
NORMALIZED OUTPUT VS VELOCITY

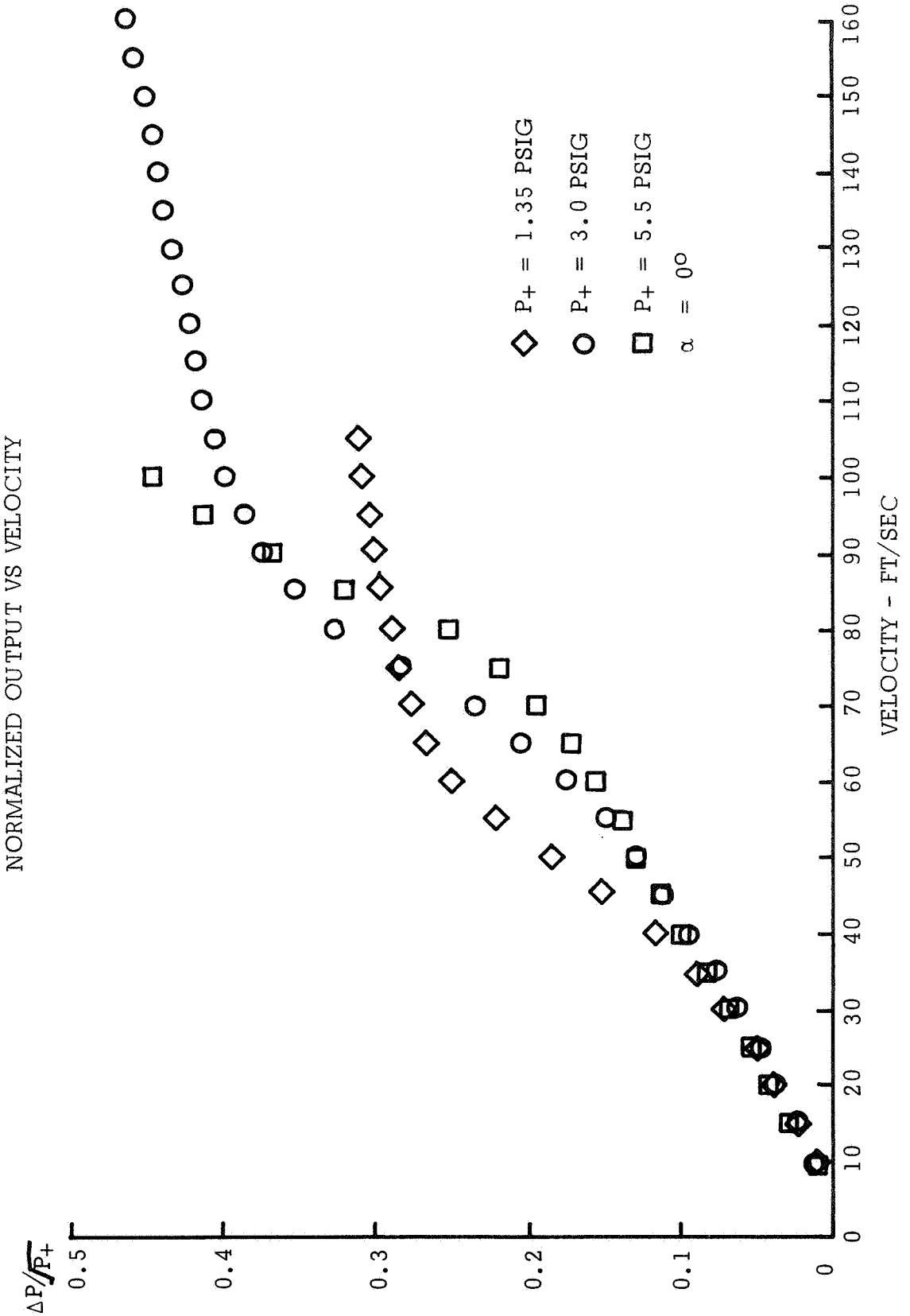

31666

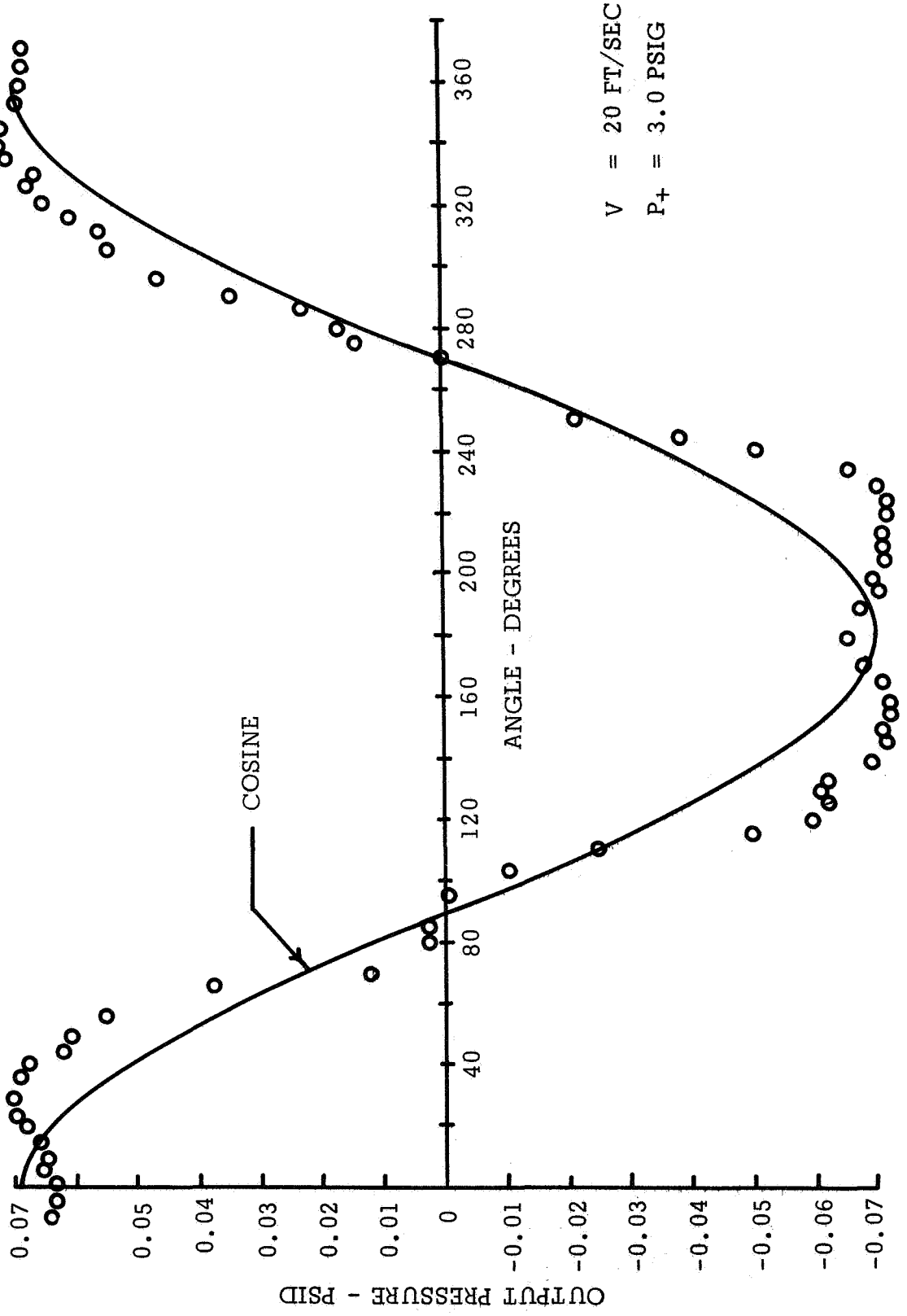

Figure 23.
OUTPUT PRESSURE VARIATION
VS
ANGLE OF ATTACK

6.0 THREE AXIS SENSOR

Figure 24 depicts a configuration for a three-axis sensor. This is a straightforward extension of the single axis sensor, and no new technical problems are anticipated. Obviously, some design is necessary to integrate the necessary flow passageways and keep weight to a minimum. The actual size of the sensor depends on the velocity threshold to be measured. This was discussed for the single axis sensor in Sections 3 and 5, and the same comments may be made in conjunction with the three-axis sensor.

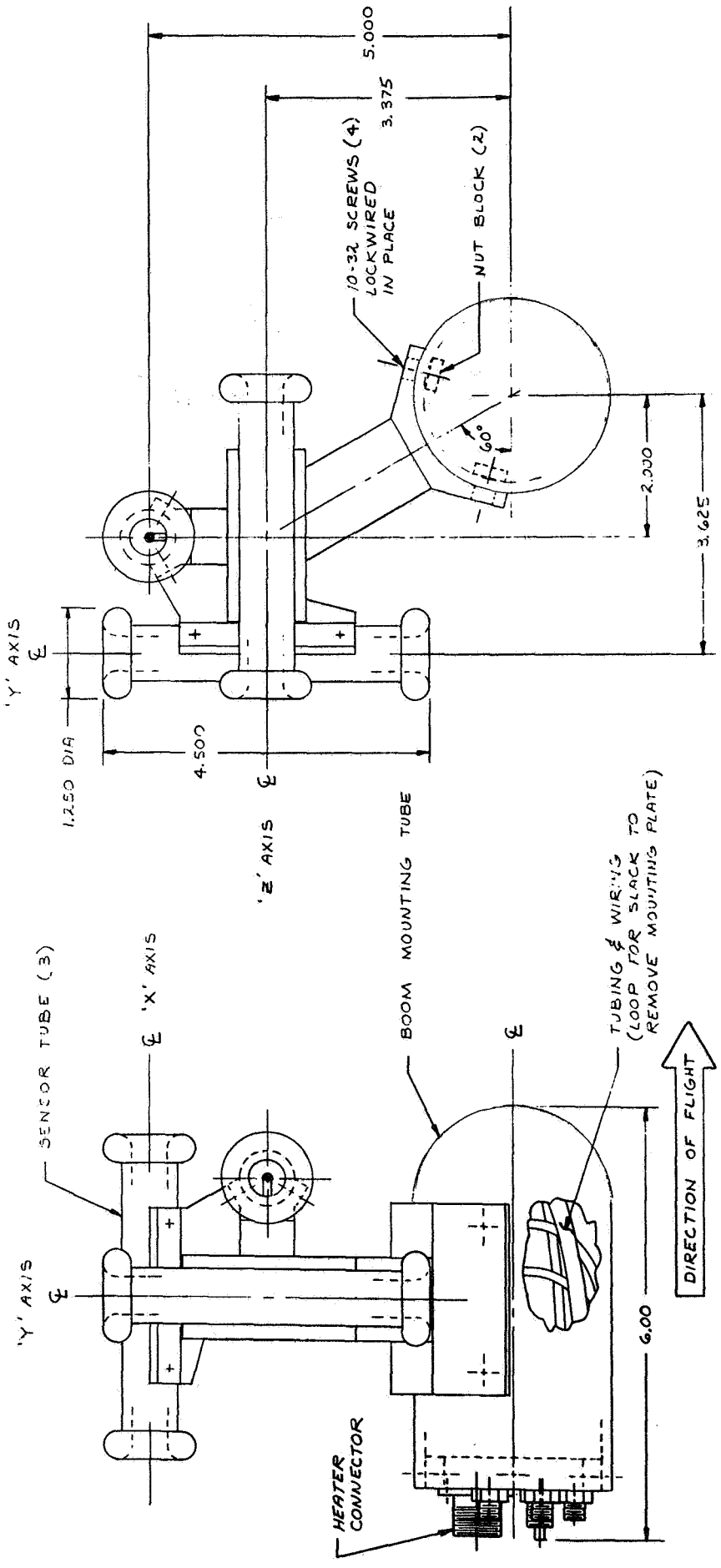

Figure 24. THREE-AXIS WIND SENSOR CONCEPT

7.0 SUMMARY

A single axis flight-worthy model wind sensor has been built and tested over the velocity range $-160 \leq V \leq 160$ ft/sec. The output has good linearity for $V < 20$ ft/sec and is quasi-linear over the entire range. The unit can provide information over total spherical coordinates. The output pressure level is high enough and may be read on conventional pressure gages or pressure transducers, even for low velocity. Low flow is required. (See Figure 15.) The unit is structurally rugged enough to withstand high speeds, and by choice of supply pressure one can utilize the "break point" (60 ft/sec in Figure 18, 90 ft/sec in Figure 19) to regulate output pressure so as to not overload the pressure transducer at high velocity. (The output pressure transducer supplied with the instrumentation may be over pressured by 100% without incurring damage.)

8.0 CONCLUSIONS AND RECOMMENDATIONS

8.1 Conclusions

Considerable development work has gone into this flight-worthy single axis fluidic wind sensor. The unit presently uniquely fills a gap in the instrumentation requirements for low speed velocity measurement.

Those attributes which make this sensor unique are its:

- Linearity
- Low velocity threshold
- High range
- High speed of response
- Ability to function in contaminated environment
- Angular resolving capability
- Inherent ruggedness and reliability
- Low cost

8.2 Recommendations

As with all instrumentation, there is always the need for further improvement. Such matters as noise, linearity, threshold, size, weight, material selection, etc., require further continual study.

Although further work should be done in these areas, the work to date has shown the potential for this instrument, even in its present state.

It has become clear during the course of this work that there is a definite need for a rugged, accurate, highly responsive low speed air speed indicator, both for aircraft needs and a variety of other applications (Reference 13). The basic simplicity, range, linearity, sizable output signal, the elimination of moving parts and the operation in adverse environments make this fluidic sensor a good competitor to other methods of low speed sensing.

9.0 REFERENCES

1. Durbin, E. J., "A Vector Airspeed Measuring System for Helicopters and Other V/STOL Aircraft", 25th Annual National Forum Proceedings, Washington, D. C., 1969.

2. Neradka, V. F. and Turek, R. F., "Fluidic Low Speed Wind Sensor Research Study", NASA CR-86352, December 1969.

3. Tanney, J. W., "An Anemometer for Very Low Velocities", National Research Council of Canada, Aeronautical Report LR-472, February 1967.

4. Carbonar, M., Colin, P. E., and Olivari, D., "The Deflection of a Jet by a Cross Flowing Stream and Its Application to Anemometry", Fourth Cranfield Fluidics Conference, 1970.

5. Tanney, J. W. and Robinson, B. R., "Performance Evaluation of a Fluid Jet Velocity Sensor With Air Supply Pressures From 15 to 700 PSIG", National Research Council of Canada Report LTR-LA-14, 1968.

6. Schlicling, H., "Boundary Layer Theory", McGraw-Hill, Inc., New York, 1960.

7. Rosenhead, L., "Laminar Boundary Layers", Oxford at the Clarendon Press, 1963.

8. Kirshner, J. M., "Fluid Amplifiers", McGraw-Hill, Inc., New York, 1966.

9. Pope, A., "Wind-Tunnel Testing", John Wiley & Sons, Inc., New York, 1954.

10. Abbott, I. H. and VonDoenhoff, A. E., "Theory of Wing Sections", Dover Publications, Inc., 1959.

11. MIL-E-5400K, Class 1A, Category 1

12. MIL-STD 454B

13. Miner, R. J., "A Fluidic Low-Speed Air-Speed Indicator", AIAA Paper No. 70-906, 1970.

APPENDIX A

ENVIRONMENTAL TESTING OF THE PARALLEL FLOW FLUIDIC WIND SENSOR

ENVIRONMENTAL TESTING OF THE PARALLEL FLOW FLUIDIC WIND SENSOR

TM-188

Work Performed Under Contract N00014-70-C-0338

by

Vincent F. Neradka

Bowles Fluidics Corporation
9347 Fraser Avenue
Silver Spring, Maryland 20910

September 1970

ABSTRACT

A Parallel Flow Fluidic Wind Sensor is wind tunnel tested in some adverse environments. A description of the test and the test results are presented.

I. INTRODUCTION

Tests of the Fluidic Wind Sensor were conducted in the closed circuit wind tunnel of Environmental Engineering Inc. of Gainesville, Florida. The sensor, which was designed and built under NASA contract NAS 12-2038, was mounted near the center of the 2 ft diameter test section. Velocity of the tunnel was set using the previously determined calibration curves supplied by Environmental Engineering, rather than actual pitot-static readings at the sensor location itself. Whereas this can cause some error in the recorded data due to nonuniformity of flow, such error is considered to be small and within engineering tolerances.

The temperature of the air in the tunnel was maintained at the operator's choice of set points by a feedback control system. Because of the soft solder (lead - tin) used in fabricating the wind sensor, an upper limit of temperature for the test was set at 300°F. The minimum temperature of the tunnel, due to viscous dissipation was slightly less than 250°F, and therefore all data are recorded at either 250°F or 300°F.

The air supplied to the wind sensor was at 90°F, the daily average for Gainesville for the days of the test. Output pressures were monitored with an electronic pressure transducer. All tests were conducted at atmospheric pressure and under continuous operation.

Solid particulate matter (glass beads up to 100μ diameter) was introduced into the flowing tunnel in amounts suggested by Environmental Engineering based on their knowledge of environmental conditions. In these contaminated tests the sensor output was monitored for two hours. Since there is a decay of contaminate with time, testing for a longer period was not considered.

Water was similarly introduced into the tunnel. This vaporized at the tunnel temperatures.

After the unit was removed from the tunnel it was disassembled for inspection. The unit, which was tested for a total of nearly 16 hours in adverse environment, showed no buildup of contaminate nor any other physical change.

II. EFFECT OF SOLID CONTAMINATE

Figure 1 shows the output pressure vs wind velocity for clean air, 1.5 grain/ft^3 and 10 grain/ft^3 solid particles. In each case the sensor output was monitored for two hours, during which no alteration in performance was observed. To attach some significance to these values, 1.5 grain/ft^3 represents a severe sandstorm, as much as 2 grain/ft^3 has been measured in air and as much as 10 grain/ft^3 may be the stack gas concentration in a fossil fuel combustion process.

III. EFFECT OF WATER VAPOR

Figure 2 shows that the water vapor had negligible effect on the sensor performance. The 10% vapor represents the moisture released in a fossil fuel plant, and the 100% vapor is simply to show that even the extreme case has negligible effect.

IV. EFFECT OF WIND STREAM TEMPERATURE

The effect of temperature was to decrease the gain of the wind sensor. Figure 3 shows the data recorded at Environmental Engineering, and also previously recorded data for a comparable test at lower temperature. Attempts are presently being made to normalize the data, thereby accounting for temperature variation without calibrating the sensor at various temperatures, but they have thus far been unsuccessful due to the difficulty of ascribing physical properties of the gas in the jet-free stream mixing region.

V. SUMMARY

It may be stated that the Fluidic Wind Sensor operates in a predictable and repeatable fashion in contaminated environments. No deterioration in performance was observed in a total of nearly 16 hours of testing.

When operating the sensor at elevated free stream temperatures, the sensor provides a repeatable output proportional to velocity. The decrease in gain necessitates calibration of the sensor at the free stream temperature, at least until the desired normalization study is successfully completed.

Figure A-1.
TEST OF WIND SENSOR IN CONTAMINATED ENVIRONMENT

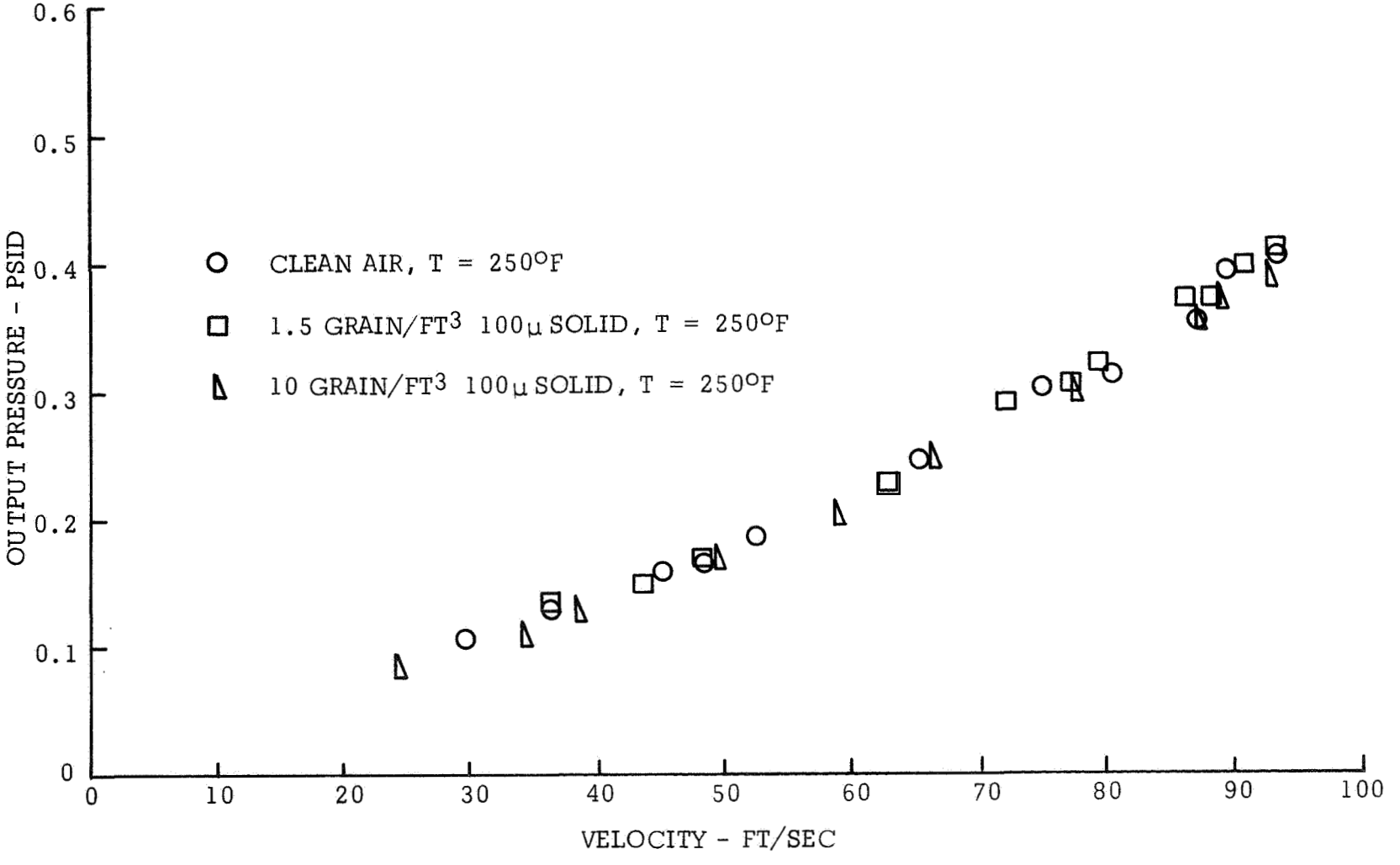

31654

Figure A-2.
TEST OF WIND SENSOR IN WATER VAPOR

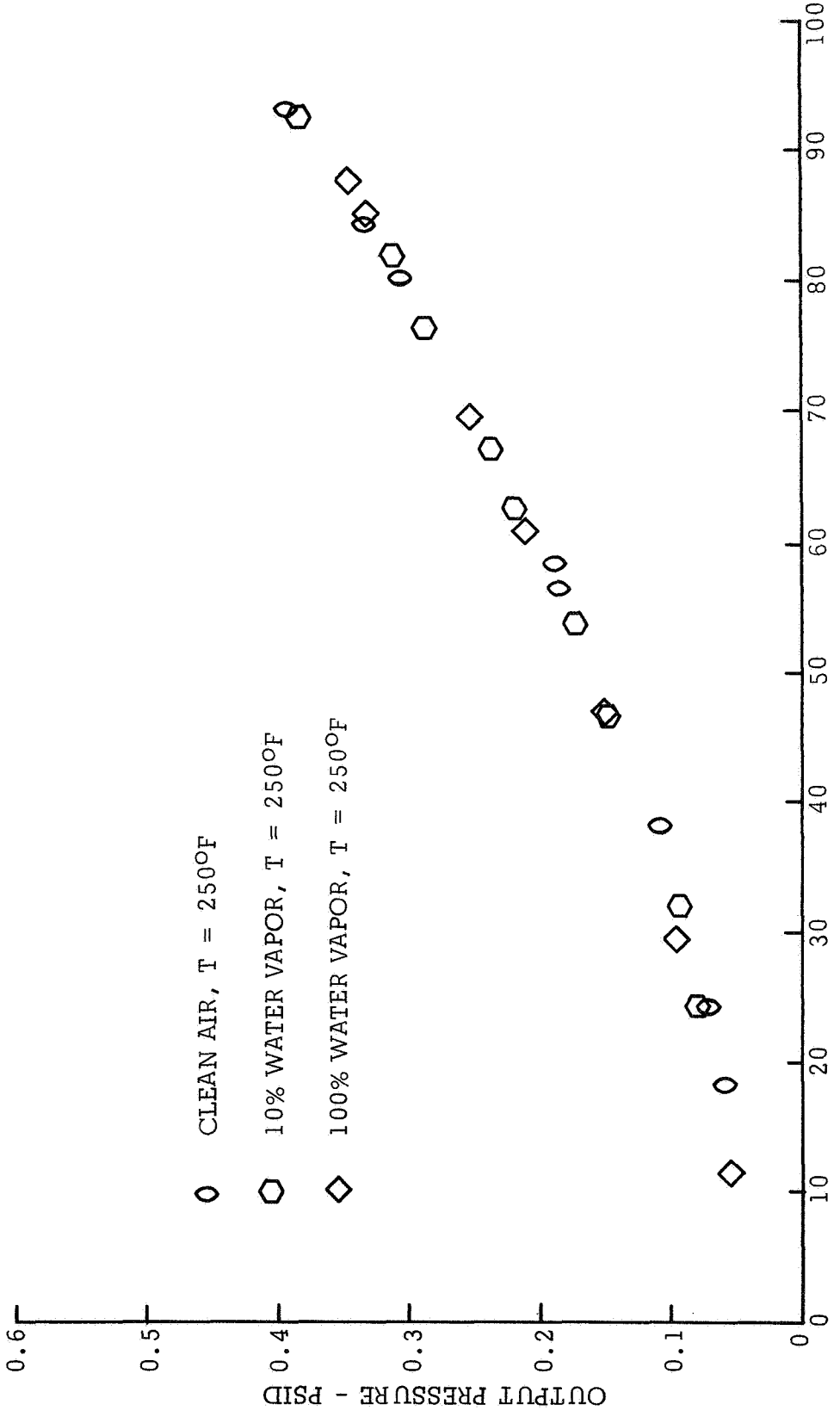

31655

Figure A-3.
TEST OF WIND SENSOR AT ELEVATED TEMPERATURE

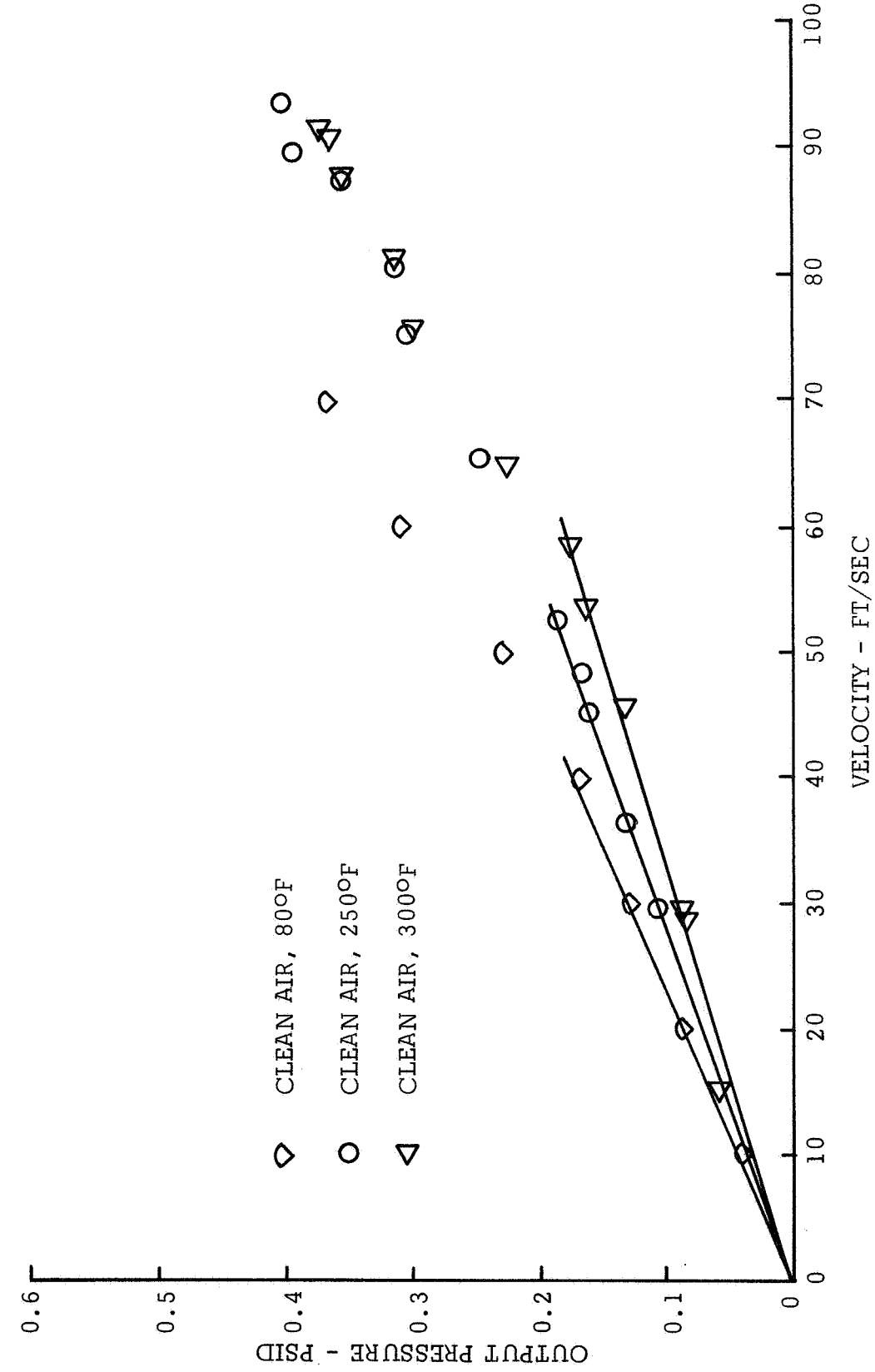

31656

APPENDIX B

NEW TECHNOLOGY

NEW TECHNOLOGY

New technology developed under this contract includes a means of null adjustment (p. 30), reduced noise (p. 11), improved angular response, inclusion of a deicer (p. 30) and extension of the basic sensor to a three axis sensor (p. 43).